FIBER OPTIC COMPASS DEVELOPMENT

A Dissertation

by

KYONGTAE PARK

Submitted to the Office of Graduate Studies of
Texas A&M University
in partial fulfillment of the requirements for the degree of

DOCTOR OF PHILOSOPHY

August 2004

Major Subject: Electrical Engineering

FIBER OPTIC COMPASS DEVELOPMENT

A Dissertation

by

KYONGTAE PARK

Submitted to Texas A&M University
in partial fulfillment of the requirements
for the degree of

DOCTOR OF PHILOSOPHY

Approved as to style and content by:

Ohannes Eknoyan (Chair of Committee)	
Chin B. Su (Member)	Robert D. Nevels (Member)
Chii-Der S. Suh (Member)	Chanan Singh (Head of Department)

August 2004

Major Subject: Electrical Engineering

ABSTRACT

Fiber Optic Compass Development.

(August 2004)

Kyongtae Park, B.S., Kangwon National University, Korea;

M.S., Kangwon National University, Korea

Chair of Advisory Committee: Dr. Ohannes Eknoyan

A fiber optic system for measuring magnetic heading and pitch of one or more compass heads in a towed acoustic array has been developed as a cooperative effort between engineers at Fiber Dynamics, Inc., and faculty and graduate students at Texas A&M.

An unconventional photolithographic process for producing a bar-code pattern on a curved (spherical) surface was successfully implemented. First, an absorption process for applying a thin layer of photoresist uniformly to the gold-coated surface of a glass sphere was perfected. Then, a system for defining the patterns in the metal was assembled. A LabView computer program controlled the system as required to define the bar code pattern in the metal. High-quality bar code patterns were produced on floating spheres by this method.

The data acquisition/signal processing system digitized and processed the raw data returning from the compass heads, and computed magnetic heading and pitch from the data. Processing of the signal from a single compass head required readout of a 7-bit

binary code giving coarse heading, using timing information to obtain fine heading, and measuring the apparent width of an analog bar to determine pitch. When monitoring multiple compass heads distributed along the fiber, a time-division demultiplexing technique was used for separating the data from the individual compass heads.

For testing the system, the cylindrical sensor head was mounted on a machinist's table for rotating it through 360° in the horizontal plane to vary the heading, and through ±10° about a horizontal axis to vary pitch. Measured resolutions of the system were 0.044º for heading, and 0.85º for pitch.

To My Family.

ACKNOWLEDGEMENTS

I would like to express my deepest gratitude to my advisor, Dr. Henry Taylor, for his support and guidance throughout my graduate study. His advice has always been helpful to break through any blocks during my research, and his generosity has made me feel comfortable in my job. I would also like to thank Dr. Ohannes Eknoyan for his kind support as my committee chair, Dr. Chin B. Su, Dr. Robert D. Nevels, and Dr. Chii-Der S. Suh for serving on my committee. Thanks to Dr. Chung E. Lee for his help and guidance as project leader and Dr. Yichao Chen and Mr. Jim Gardner for their friendship and cooperation on the project. Thanks to Mr. Robert A. Atkins for his technical support in the lab. Thanks to all the students in our lab who have been friends all the way through my graduate study.

I would like to thank my uncle, Dr. S. B. Cho, who always showed me vision. Dr. Jinseob Eom deserves my special thanks for his endless support and guidance. I would like to thank my parents who are revered and the greatest shelter for my life and my wife, Kyonghye, for her love and faith and for standing firm by me.

TABLE OF CONTENTS

Page

Page

LIST OF FIGURES

Page

Page

Page

LIST OF TABLES

Page

I. INTRODUCTION

I. A. The Need for Hydrophone Location Information in Towed Acoustic Arrays

Beamforming of signals from towed-array hydrophones has long been a critical aspect of ocean surveillance for the navies of the world. Optimal performance for detection and tracking requires a knowledge of the exact position of each hydrophone on a three-dimensional spatial grid. Under ideal conditions, in which the towing ship or submarine is traveling in a straight line at constant depth and speed and no ocean currents are present, the cable deploys in almost linear fashion and array element locations can be accurately determined. However, when the towing vessel is maneuvering and/or strong currents are present, the cable trajectory will deviate substantially from a straight line, and coordinates of the array elements assumed by the signal processing algorithm will differ significantly from their actual locations. Unless precise information on hydro-phone location is available, beamforming performance degrades under non-ideal conditions.

I. B. Fiber Optic Heading Sensors for Towed Arrays

Since the early 1980's, the U. S. Navy has been interested in fiber optic heading sensors for towed arrays as a basis for more accurate determination of hydrophone location. Both gyroscopes and magnetometers have been considered, but neither

---

This dissertation follows the style and format of *IEEE Journal of Lightwave Technology*.

technology has yet proven practical for this application. In the case of the gyroscope based on the Sagnac interferometer, the requirements for small size, low power consumption, high accuracy without calibration over an extended time period, and low cost have been major impediments.

Several approaches to a three-axis fiber optic magnetometer are possible. A magnetic field component along the axis of a fiber causes a rotation of the plane of polarization of propagating light via the Faraday effect, which has been known since the 19th century. Unfortunately, many meters of fiber are required to sense the earth's magnetic field, so Faraday-effect sensors are not consistent with the dimensions specified by the Navy. Fiber Dynamics, Inc., has built small (1 cm long by 0.4 cm diameter) single-axis magnetometers in which a very slight motion of a permanent magnet produces strain in a fiber Fabry-Perot interferometer [1]. This "FFPI magnetometer" is, in principle, sensitive enough to measure the earth's field, but we believe that 3 magnetometer axes and 3 accelerometer axes will be needed to implement the Navy system. In such a system, the effects of thermal drifts and cable acceleration are major concerns, the mechanical design of the sensor head as well as the signal processing are rather complex, the cost is projected to be high, and up to 6 fibers would be needed in the tow cable for each fiber optic compass.

The most commonly investigated approach to the fiber optic magnetometer is based upon the magnetostrictive effect, in which an applied magnetic field induces a dimensional change in a ferromagnetic material [2-5]. In implementing a fiber optic magnetometer based on this principle, a single mode optical fiber coated with nickel [6]

or wrapped around a Metglas cylinder [7] experiences a strain which is dependent on the external magnetic field [8-10]. The fiber is deployed in one arm of a Michelson or Mach-Zehnder interferometer, such that the optical output from the interferometer is modulated in response to a change in the magnetic field. The same drawbacks mentioned above for the FFPI magnetometer (the need for up to 6 single-axis sensors per compass, erroneous readings due to thermal drift and cable acceleration, complex mechanical design, high cost, and the need for multiple interconnecting fibers in the cable) will also apply to fiber magnetometers based on the magnetostrictive effect. None of the conventional fiber optic heading sensor approaches appears to be practical for the towed array application.

I. C. Floating Sphere Approach to Fiber Optic Compass

An alternative means of meeting the Navy's requirement - a conventional magnetic compass with remote readout using fiber optics - is being pursued by Fiber Dynamics, Inc., of Bryan, TX, and the Electrical Engineering Department at Texas A&M. The system configuration for a system for monitoring a single sensor head is illustrated in Fig. 1-1. A sensor head located in the tow cable is connected by a single fiber to the signal conditioning unit (SCU) on the ship. The SCU contains a laser light source which is scanned in frequency. A modulated light signal transmitted back to the SCU from the sensor head contains information from which its magnetic heading, pitch, and roll can be determined.

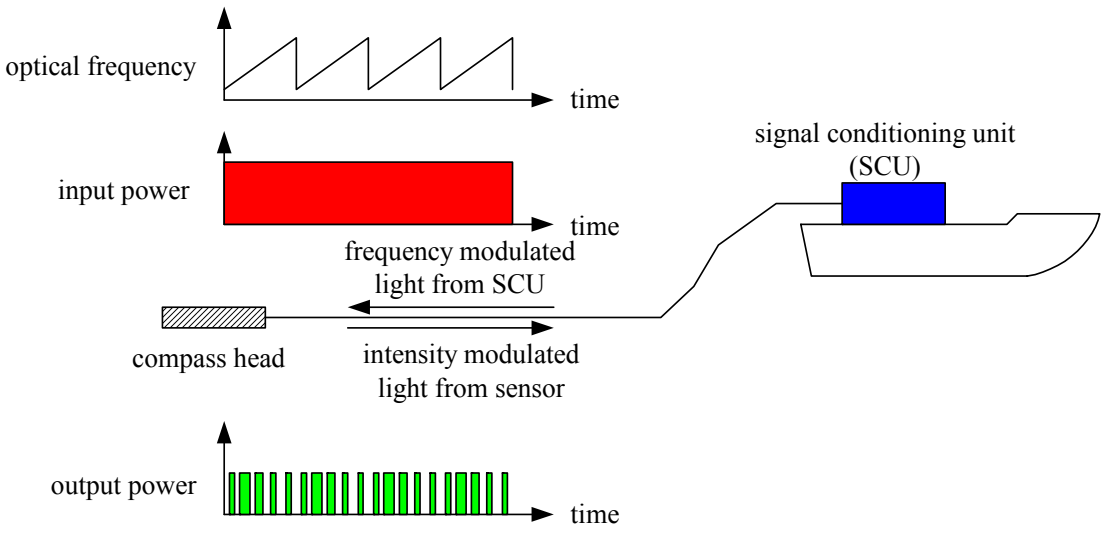

Fig. 1-1. System configuration for monitoring a single sensor head

The basic concept of Fig. 1-1 can be extended to the monitoring of many sensors arranged along the length of a single fiber through the use of time-division multiplexing, as in Fig. 1-2. To achieve this result, the frequency-scanned light source in the SCU is pulse-modulated and the return pulse from each sensor head is digitized and processed to determine its magnetic heading, pitch, and roll. The time between updates in the sensor data equals of the order of 1 s (corresponding to a 1 Hz update rate). The light source is modulated to produce microsecond-wide pulses at a much higher rate, in the 100 kHz range. Thus, many pulses are transmitted to each sensor head during each frequency scan of the broadband light source.

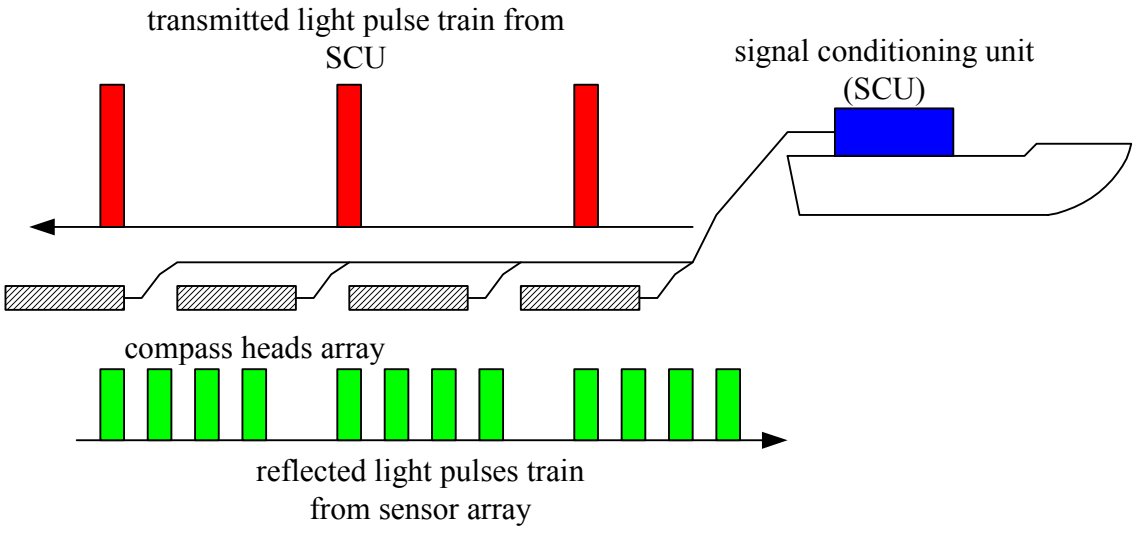

Fig. 1-2. Concept of time-division-multiplexed fiber optic compass system

Attractive features of the time-division-multiplexing approach include:

- Only one fiber is needed to connect multiple compass heads to the dry-side signal conditioning unit, thus minimizing space and connector requirements in the tow cable.
- Only one light source, one photodetector, and one signal processor are needed to operate many sensor heads, leading to cost savings in the SCU.
- Fast update rates (1 Hz or faster) are readily achieved.
- All sensor heads can be identical.
- The system is readily expandable to accommodate 6 sensor heads, to meet the Navy's requirements.

A more detailed description of the two main elements of the fiber optic compass system, the sensor head and the SCU, is given in the next two sections.

II. SENSOR HEAD DESIGN

II. A. Floating Sphere

The heart of our sensor head design is a permanent magnet mounted inside a "floating sphere (FS)", which topologically is a spherical surface near the equator and flattened at the poles. A three-dimensional illustration of FS is given in Fig. 2-1, and a schematic illustration of the mounting arrangement is given Fig. 2-2. The FS, with longitudinal markings crossing its equator to indicate its angular orientation, is mounted in a bearing assembly so that it can rotate freely about a vertical axis. A permanent magnet is bonded below the geometrical center of the FS. Thus, the FS is mechanically asymmetric, with its center of gravity (c. g.) displaced from its physical center in the direction of the magnet's c. g. The vertical is defined by a vector passing through the physical center of the FS and the c. g. of the magnet. The magnet is mounted such that its magnetization vector lies in the horizontal plane. The orientation of the FS is thus determined only by the earth's magnetic and gravity fields, and is not affected by rolling or pitching of the sensor housing.

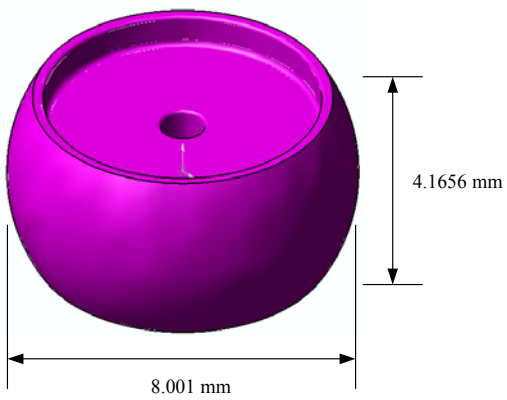

Fig. 2-1. Three-dimensional drawing of the FS

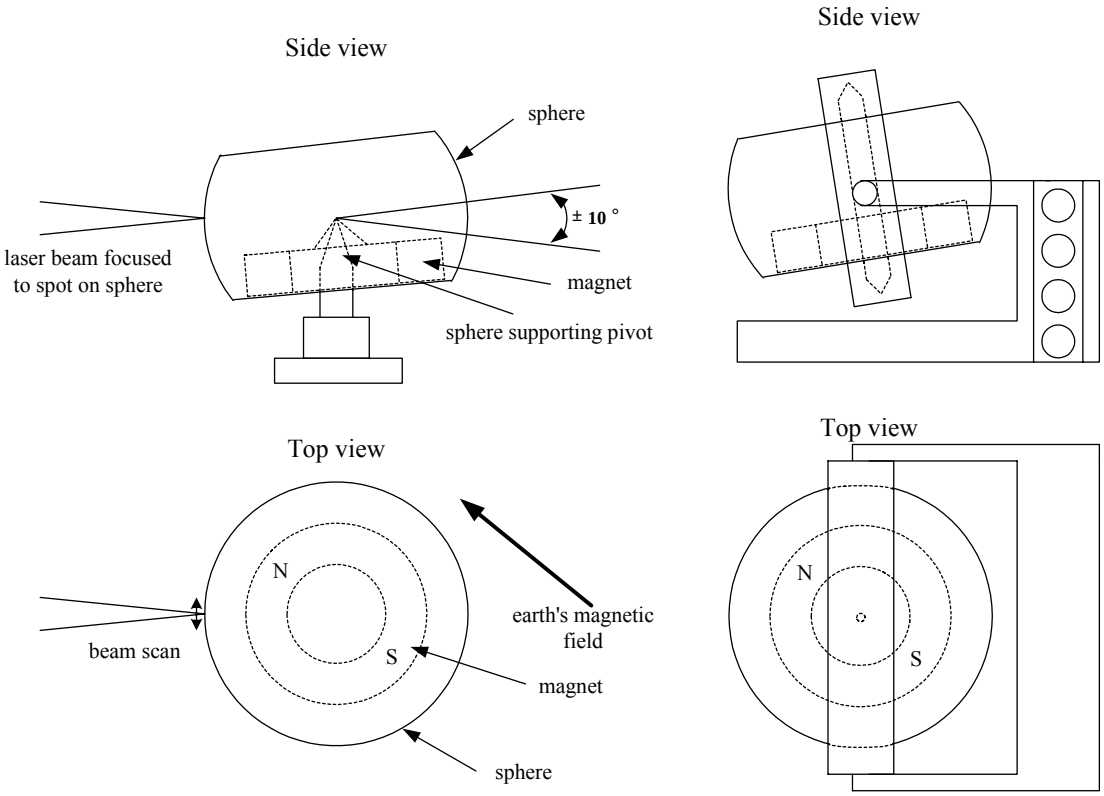

Fig. 2-2. Mounting arrangement for an FS supported by a single pivot

II. B. Sensor Head Configuration

A flying spot barcode scanner illustrated in Fig. 2-3 is used to determine the angular orientation of the FS. Scanning is accomplished using a laser light source, tunable from 1525 to 1565 nm, in the signal conditioning unit (SCU) at the dry end of the cable, in conjunction with a lens and grating in the sensor head. A single fiber transmits light from the laser to the sensor head, and return light from the sensor head to the SCU. Laser light exiting the fiber is collimated by the lens, diffracted by the grating, and focused by the lens to a small spot on the outer surface of the FS. As the laser frequency is scanned, the diffraction angle also changes and the focused spot moves on the surface of the FS in a direction parallel to the equator. Light backscattered from a barcode pattern on the surface of the FS is collimated by the lens, diffracted by the grating, and focused by the lens into the fiber, which then carries the modulated light back to the SCU.

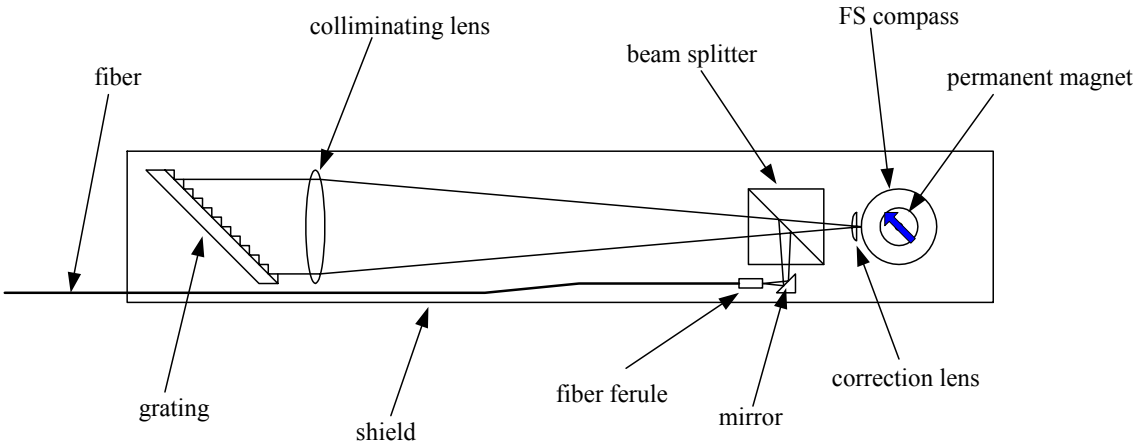

Fig. 2-3. Sensor head configuration

The grating must be maintained with its lines (rulings) in the vertical direction to match the orientation of the lines in the bar code in the floating inner sphere. This is accomplished by mounting the grating in a ring bearing assembly consisting of an inner ring which rotates freely inside an outer ring, which is attached to the sensor housing. The rotation axis of the inner ring, to which the grating is attached, coincides with the axis of the sensor housing. The inner ring is weighted at the bottom so that gravitational force maintains a vertical orientation of the lines in the grating. After the optical components are mounted and aligned on the chassis, it is inserted into pressure proof cylinder. Fig. 2-4 shows three-dimensional drawings of the sensor head seen at different angles.

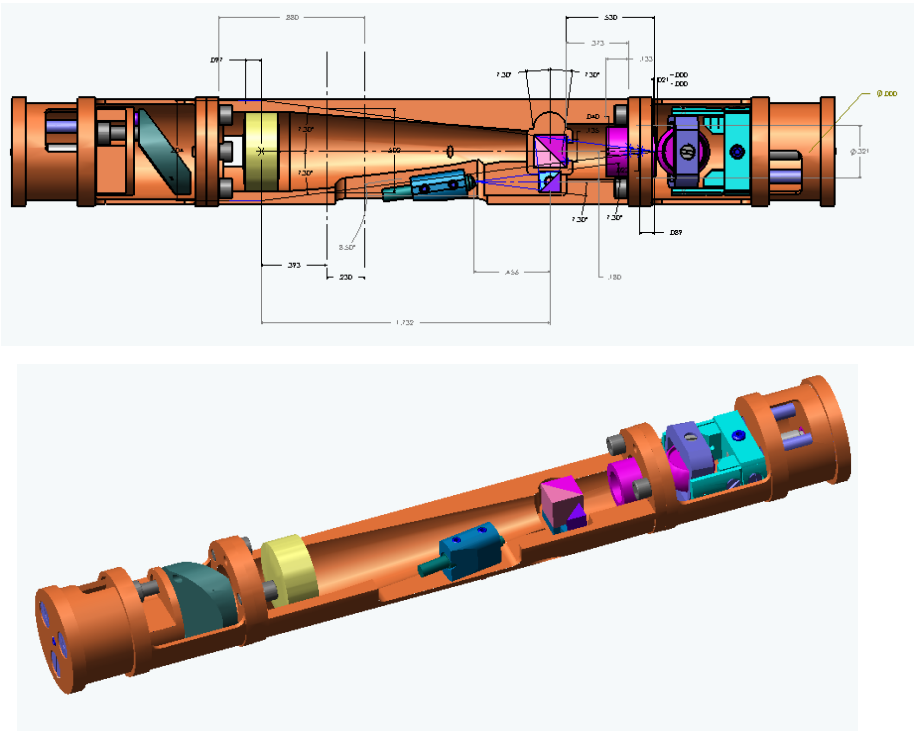

Fig. 2-4. Three-dimensional drawing of sensor head

II. C. Scanning Range

The grating equation is given by

$$\sin\theta_m - \sin\theta_i = m\frac{\lambda}{d} \qquad (2.1)$$

where θ_m is the angle of reflection, θ_i is the angle of incidence, m is the order, λ is the wavelength and d is the grating pitch. We used a grating with 600 lines/mm, so d = 1666 nm. The angle of incidence of light impinging on the grating should be the same as the angle of reflection in order to couple back the barcode scanned light to the fiber. Assuming that the grating is used in the first order, equation (2.1) becomes

$$2\sin\theta_i = \frac{\lambda}{d}. \qquad (2.2)$$

The sketch in Fig. 2-3 then simplifies to Fig. 2-5. It follows from eq. (2.2) that θ_i = 27.71° for λ = 1550 nm and d = 1666 nm, and that the range of θ_i is 0.78° for a wavelength scan from 1525 nm to 1565 nm. Furthermore, as illustrated in Fig. 2-6, the corresponding range R of the scan on the surface of the FS is

$$R = 50\tan^{-1}(0.78°) = 0.68 \text{ mm} \qquad (2.3)$$

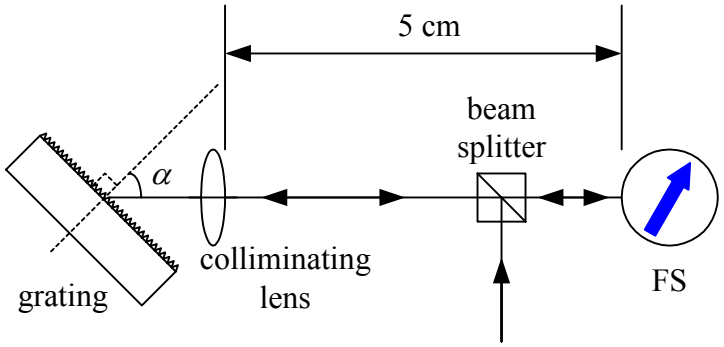

Fig. 2-5. Reflection grating

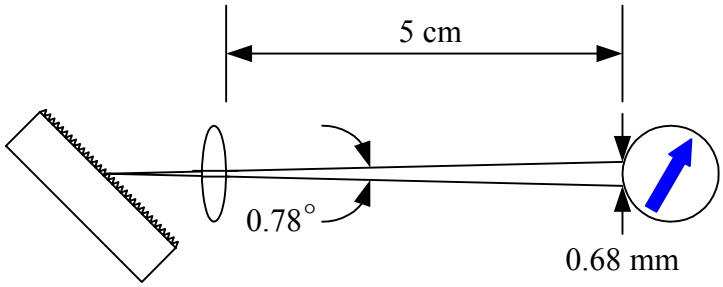

Fig. 2-6. Scanning diagram

II. D. Correction Lens

There is a substantial power penalty in scanning the FS barcode pattern due to the fact that off-axis rays do not reflect back along the incident optical path, as illustrated in Fig. 2-7. This leads to a mismatch between the reflected mode electric field amplitude distribution vs. the amplitude distribution which corresponds to the fiber mode.

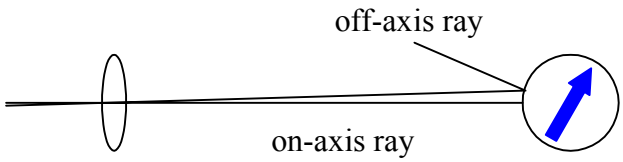

Fig. 2-7. Reflected ray traces from FS

As a solution, a correction lens of short focal length is inserted near the FS, as in Fig. 2-8.

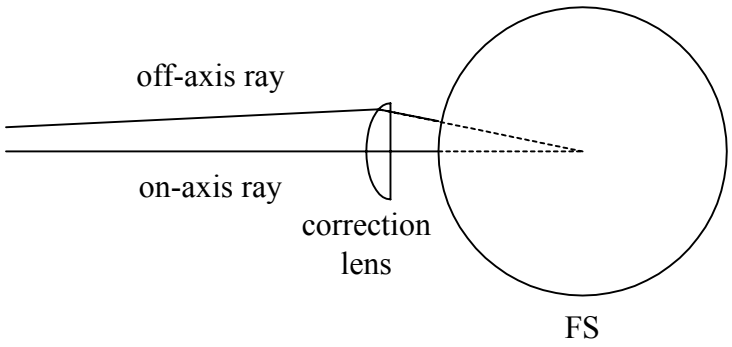

Fig. 2-8. Correction lens

The focal length of the correction lens is close to the radius of curvature of the FS (4.0005 mm) so that the incident rays impinge on the surface of the FS at normal incidence, and are therefore reflected back along the incidence path.

II. E. Barcode Pattern

A flat projection of a portion of the bar code pattern is illustrated in Fig. 2-9. Bars in the code are oriented perpendicular to the equator. Angular orientation (heading)

is indicated by 80 code words arranged consecutively around the circumference of the sphere, 360 º/80 = 4.5 º per word. Each word is uniquely identified by a seven-bit binary code. In addition, each word contains a “fat one” 1.5 bit periods wide, a “fat zero” 1.5 bit periods wide, and a triangular analog section 3 bit periods wide. The “fat one” followed by a “fat zero” is provided as a unique indicator of the end of a seven-bit binary sequence.

The optical signal from the sensor heads, containing the scanned barcode information, is converted to an electrical signal by a photodetector and processed digitally to determine the sensor head orientation relative to the earth's magnetic and gravity fields. Coarse magnetic heading is determined by reading the barcode. Fine magnetic heading is determined by measuring the time from the initiation of a frequency scan until a transition ("0" to "1", or "1" to "0") occurs.

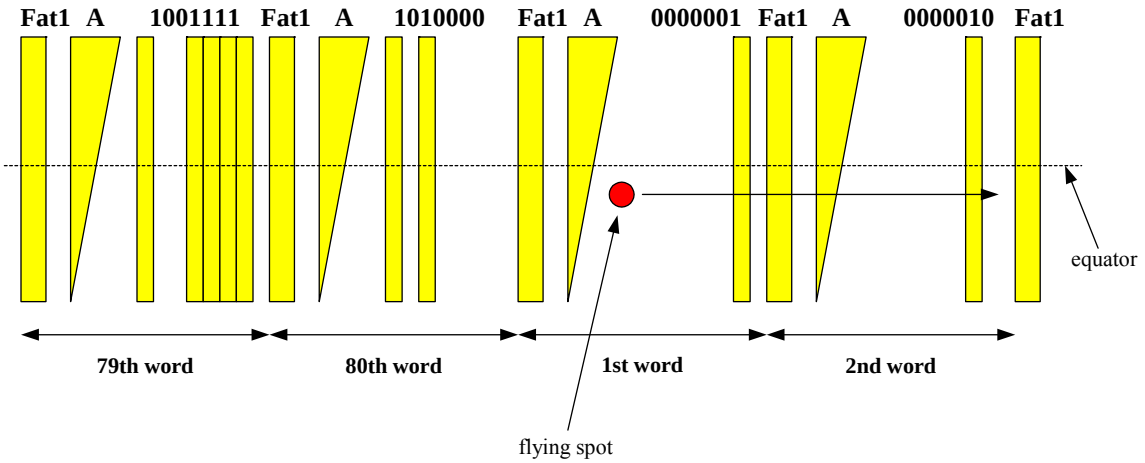

Fig. 2-9. Barcode pattern with tapered gaps for determining pitch as well as heading

The ability of the system to determine pitch as well as magnetic heading makes use of the fact that the latitude of the focused spot on the outer surface of the inner sphere is equal to the pitch of the sensor head. Our scheme for measuring the pitch introduces a triangular analog section in each word of the bar-code pattern. The width of this analog section varies linearly from top to bottom over the range of latitudes from -10° to +10°. Thus, the temporal width of the optical modulation produced by scanning of the flying across spot across an analog section varies in proportion to the latitude.

A barcode pattern for 80 words is illustrated in Fig. 2-10. Because 1 word contains 15 bit periods, the total number of bit periods is 1200. The height of the pattern is 1.4 mm, which equals 20° in pitch angle. One bit period, the width of a binary "zero" or "one", is 21 μm, which equals to 0.3° in heading angle. The width of one word is 15 x 21 μm = 315 μm = 0.315 mm. Since the scanning range is 0.68 mm, more than 2 words are contained within each scan.

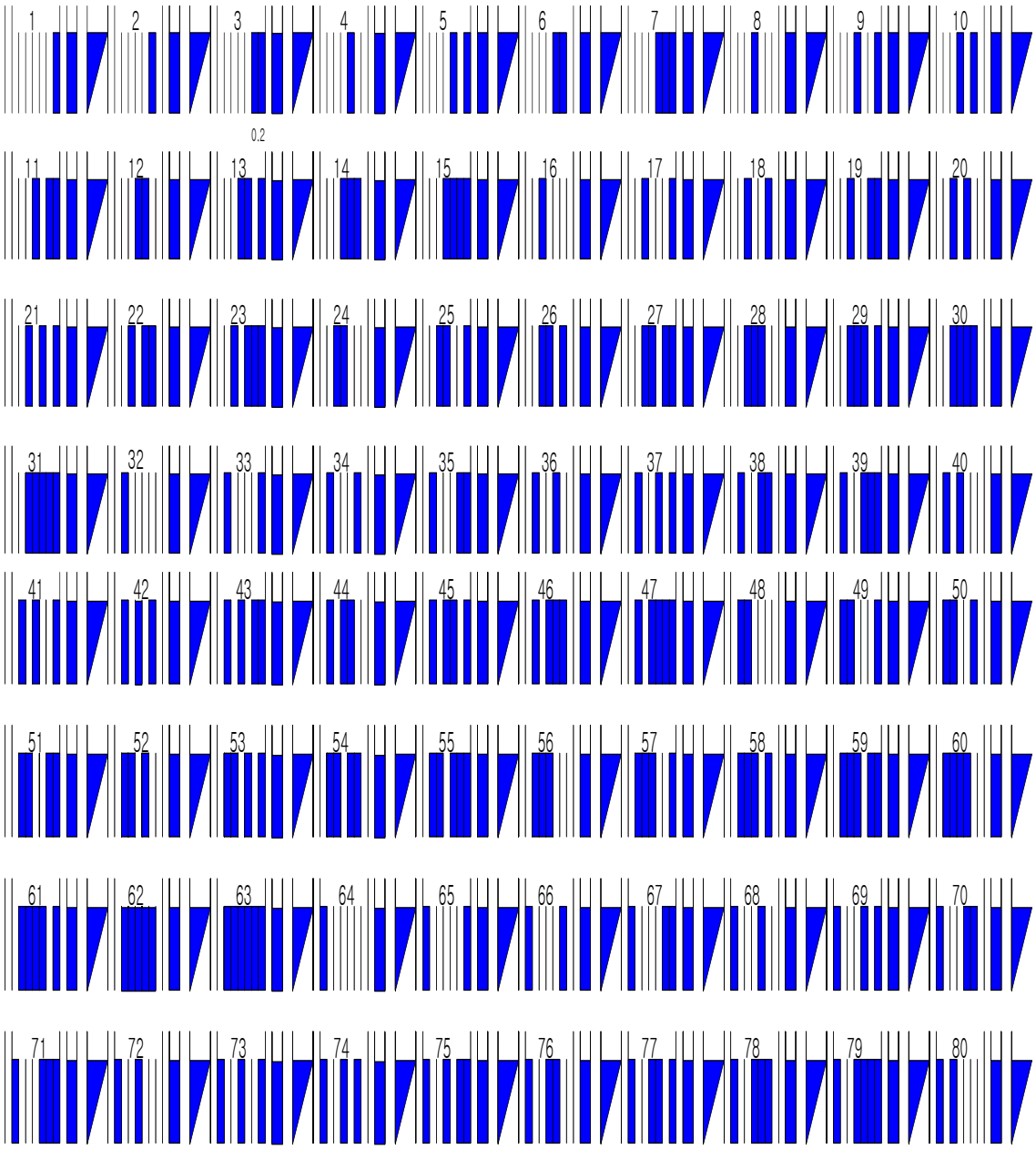

Fig. 2-10. Barcode pattern for 80 words

III. SIGNAL CONDITIONING UNIT (SCU) DESIGN

The SCU is illustrated schematically in Fig. 3-1. The light source is an erbium doped fiber (EDF) laser in the ring configuration [11-12]. Total amplified spontaneous emission (ASE) power is 7 mW at 45 mW pump power. The laser is spectrally scanned in the 1525 ~ 1565 nm range using a grating and a rotating mirror, with a single mode fiber serving as a spatial filter and collecting the light reflected by the mirror. By adjusting the ramp signal amplitude and offset of mirror scanning, the laser wavelength is tuned over the entire EDF gain region. As the mirror rotates, the frequency of light coupled into the fiber core changes. The power spectrum at 6 different wavelengths was measured with 0.1 nm spectral resolution, as illustrated in Fig. 3-2.

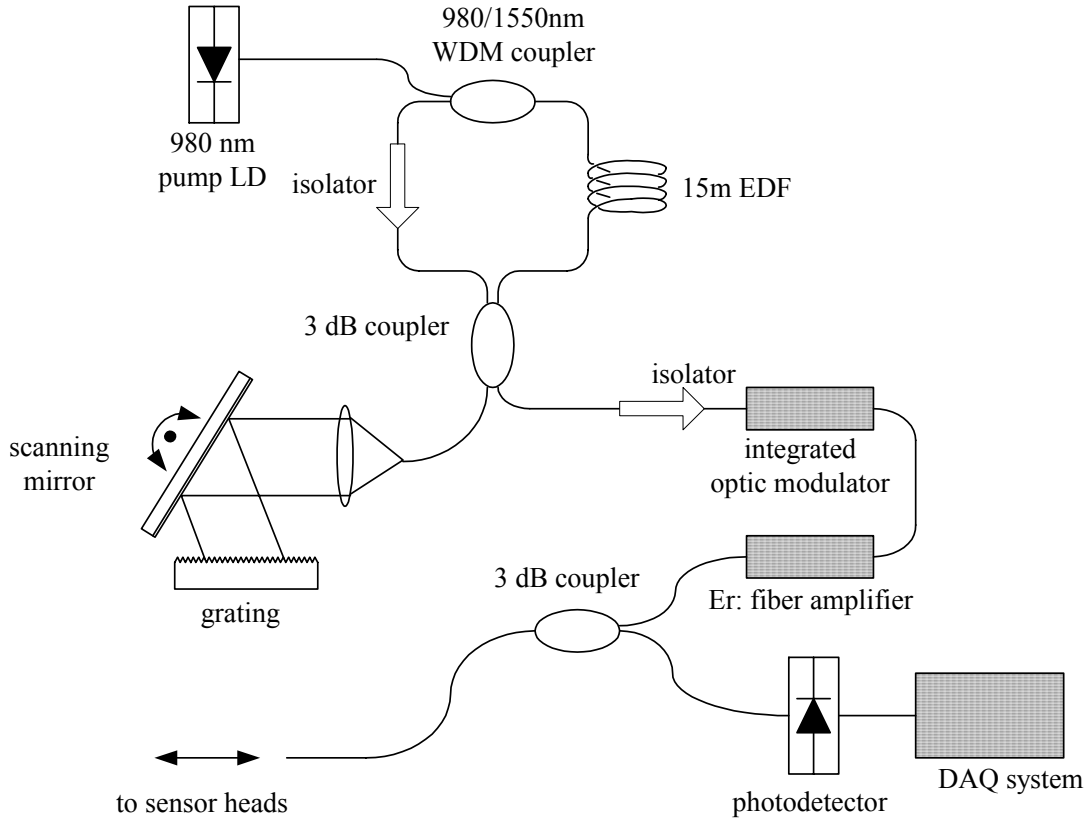

Fig. 3-1. Dry-end SCU

The laser power variation over the scanning range is less than 5 dB, and the ratio of laser power to ASE power is > 20 dB in the scanning wavelength region.

To implement time division multiplexing, the light collected by the fiber is pulse modulated by an integrated optic modulator and amplified by a commercial erbium-doped fiber amplifier (EDFA). The spectrum of the laser after amplification at 6 different wavelengths is shown in Fig. 3-3. After amplification, the light passes through a fiber coupler to the array of optical compass heads.

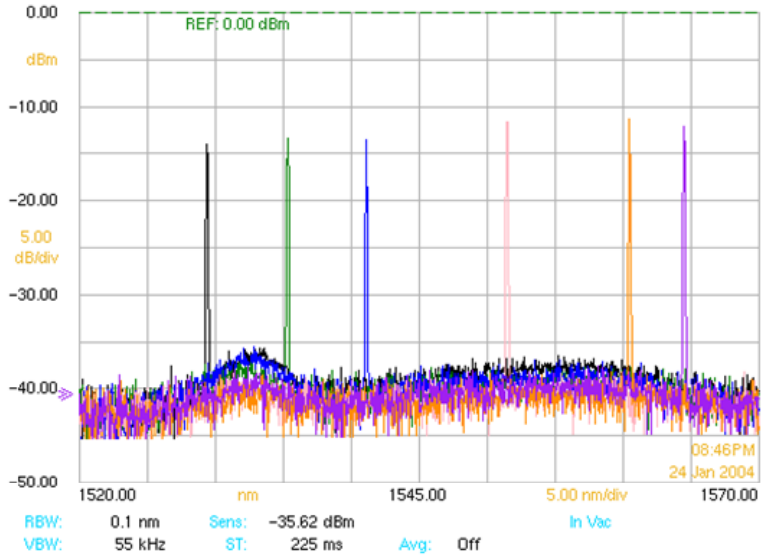

Fig. 3-2. Spectrum profiles captured at 6 different laser wavelengths

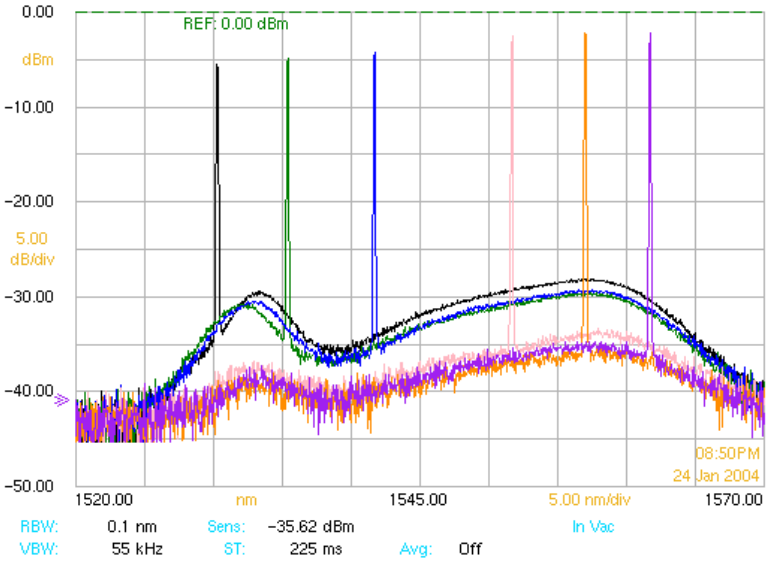

Fig. 3-3. Spectrum profile after EDF amplifier

The gain of the EDFA is ~20 dB. The optical modulator is driven by a rectangular wave with 10 % duty cycle. The temporal dependence of the broadband light source pulses and of the returned pulses from the sensor heads are illustrated schematically in Fig. 3-4. The pulse repetition frequency is 100 kHz. The duty cycle is 10 % so that the pulses are separated by 10 μs. The 1.5 μs spacing between signal pulses is determined by the optical transit time corresponding to the 150 m spacing between compasses in the array. This 1.5 μs figure also represents the maximum allowable pulse width. The minimum pulse spacing for a 6-compass array would be 6 x 1.5 μs = 9 μs. Thus, the pulse repetition frequency would need to be less than 111 kHz.

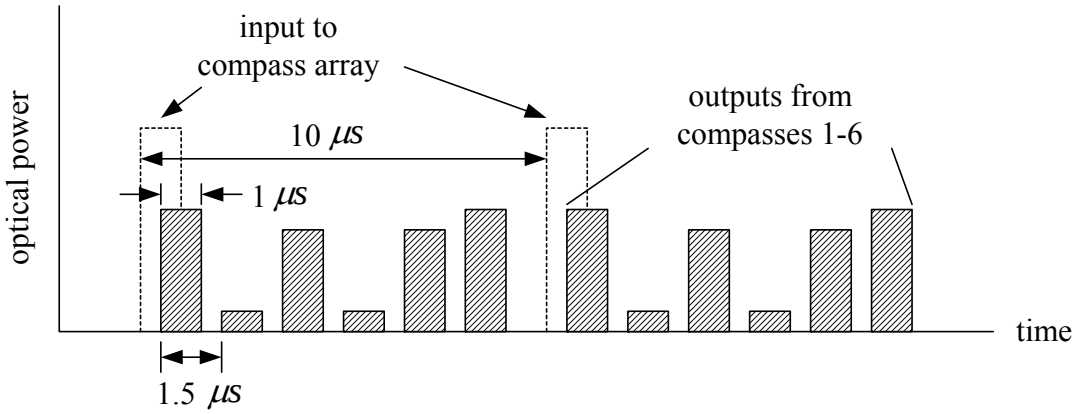

Fig. 3-4. Schematic illustration of input and output light pulses in temporal domain

The system is designed to produce about 100 resolvable spots in the 1525 - 1565 spectral range, and the number of illuminated rulings in the grating is about 5000. The baseline scan rate for the mirror is 1 Hz, which corresponds to the rate at which sensor information on heading and pitch is updated. Faster update rates are readily achievable if needed.

IV. OVERVIEW OF DISSERTATION RESEARCH

Development of the fiber optic compass system described has involved the efforts of engineers at Fiber Dynamics as well as faculty and graduate students at Texas A&M. The work described here addresses three key aspects in the development:

Task A. Fabrication of the bar code pattern on the floating sphere - a novel lithography system for producing patterns for the floating spheres used in the compass heads was designed and implemented in the Solid State Laboratory of the Electrical Engineering Department at Texas A&M. This research is described in section V.

Task B. Data acquisition/signal processing - The electrical signal from the photodetector in the SCU was digitized, and the signal processor converts these raw optical data to readings of angular orientation and pitch of the sensor heads - one set of optical readings for each spectral scan of the laser. This research is described in section VI.

Task C. System testing and performance verification - To test the system and verify the utility of the bar code patterns (Task A) and the data acquisition/signal processing technique (Task B), the sensor head was mounted on a machinist's table for rotating its heading through 360° in the horizontal plane, and its pitch through ±10°. Data collected

for different orientations of the sensor head were compared with actual heading and pitch to determine the system's performance. This research is described in section VII.

V. FABRICATION OF BAR CODE PATTERN ON A FLOATING SPHERE

Producing a mask of a pattern such as a barcode and reproducing it photolithographically on a flat surface is a routine task. However, making such a pattern on a curved (spherical) surface is not standard in industry. Despite several attempts, no vendor could produce a satisfactory result. For that reason, the patterns for the FSs used in the compass heads was produced in the Solid State Laboratory of the Electrical Engineering Department at Texas A&M using unconventional techniques for both application of the photoresist and lithographic exposure of the barcode pattern.

V. A. Lithography System Design

The system for defining the barcode patterns on the surface of a gold-coated FS illustrated in Fig. 5-1 [13]. It consists of a high precision (.001°) computer-controlled rotation stage, a mask holder to accommodate a rectangular mask or a triangular mask, a lens for producing a 10x reduced image of a mask onto the surface of the floating sphere, a light source for illuminating the mask in transmission, and a computer-controlled shutter for blocking the light. A Labview computer program controls the rotating stage and shutter as required to define the pattern in the metal.

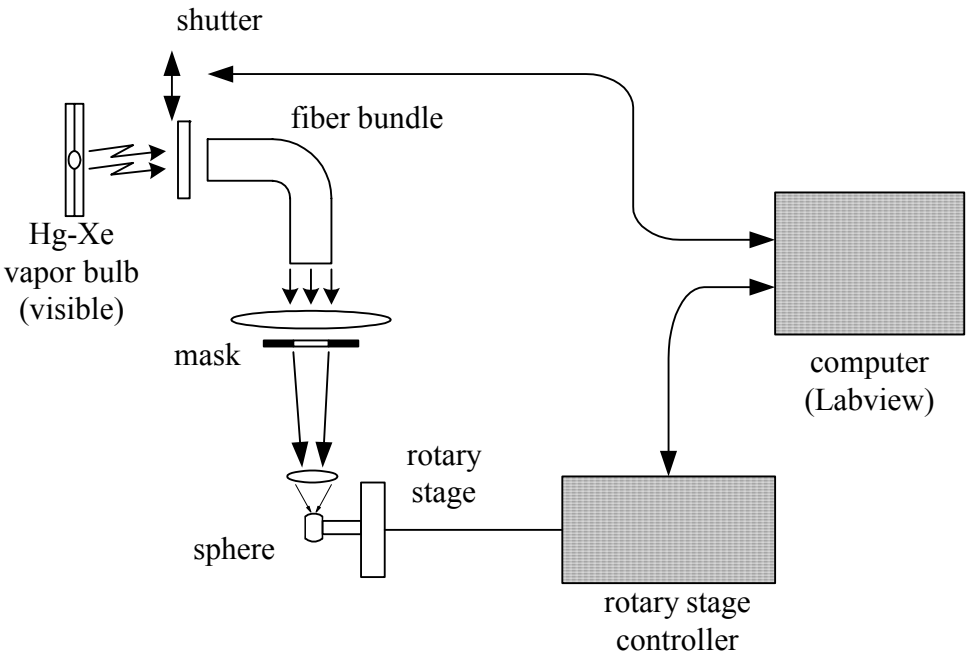

Fig. 5-1. Arrangement for photolithographic definition of digital and analog patterns on a FS

V. B. Process for Producing the Patterns

The process steps for producing a pattern on an FS are:

1. Coating the glass FS with gold
2. Applying photoresist uniformly on the surface of the FS
3. Stabilizing the photoresist by baking
4. Closing the shutter
5. Turning on the light

6. Mounting the FS on the rotation stage such that the polar axis of the FS coincides with the stage's rotation axis
7. Inserting the mask containing the rectangular aperture into the mask holder
8. Rotating the stage under computer control to the position of a "one" in the pattern
9. Opening the shutter under computer control to expose the resist
10. Closing the shutter
11. Repeating steps 8 - 10 until all of the "ones" have been produced, corresponding to 360° rotation of the stage
12. Inserting the mask containing the triangular aperture into the mask holder
13. Rotating the stage under computer control to the position of an "analog section" in the pattern
14. Opening the shutter under computer control to expose the resist
15. Closing the shutter
16. Repeating steps 13-15 until all of the "analog sections" have been produced, corresponding to 360° rotation of the stage
17. Removing the FS from the rotating stage
18. Developing the exposed resist
19. Etching the FS in aqua regia to define the bar code pattern in the gold
20. Removal of the resist.

The FS is now ready for use in a compass head.

V. C. Shutter Control

To open the mechanical shutter in Fig. 5-1 requires > 200 mA of electrical current. To generate such big current a shutter controller circuit was inserted between a Labview data acquisition (DAQ) card and the shutter. A digital current pulse from the DAQ controlled by a Labview program is amplified by a bipolar transistor circuit (Fig. 5-2) to generate the required current. When the digital input goes back to zero voltage level the current returns to zero and the shutter closes. The shutter is opened during exposure for 10 s and closed while the rotary stage is in motion.

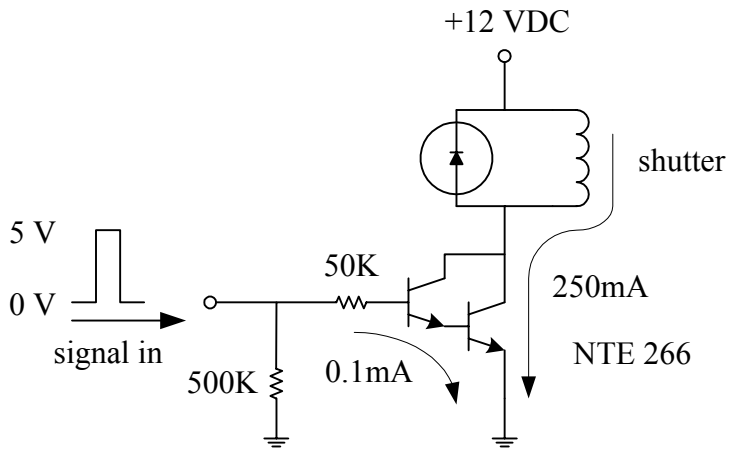

Fig. 5-2. Shutter control circuit

V. D. Rotation Control

For rotation control we used high precision (.001°) computer-controlled rotation stage. As we saw in Section II. E., each bit period in the bar code pattern subtends to

0.3° of the 360° circumference of the sphere, and each word in the pattern contains 15 bit periods and subtends 4.5°. Table 5-1 shows the rotation angles in degrees for producing the digital part of the 80-word barcode pattern with the 1-bit rectangular mask. Thus, 406 steps of the rotation stage are needed to produce the digital pattern. An additional 80 steps are needed to produce the analog pattern with the triangular mask. Each step takes 20 sec., 10 sec. for exposure and 10 sec. for rotating and settling of the stage. The entire exposure process takes ~3 hrs. After a 360° rotation, the accumulated angular error is less than 0.015°, or 5 % of 1 bit period.

Table 5-1. Rotation steps in degrees to produce the binary part of the pattern

0th to 10th	11th to 20th	21st to 30th	31st to 40th	41st to 50th	51st to 60th	61st to 70th	71st to 80th
3	0.15	2.55	2.55	2.25	2.25	2.25	1.95
0.6	2.85	0.6	0.3	0.6	0.3	0.3	1.2
0.15	0.3	0.6	0.3	0.9	0.9	0.3	0.3
3.45	1.2	0.6	0.3	0.6	0.3	0.3	0.3
0.9	0.15	0.15	0.3	0.15	0.6	0.6	0.6
0.15	2.85	2.55	0.6	2.25	0.15	0.6	0.15
3.45	0.3	0.6	0.15	0.6	2.25	0.15	1.95
0.3	0.6	0.3	2.25	0.6	0.3	2.25	0.9
0.6	0.6	0.9	2.1	0.9	0.6	0.3	1.5
0.15	0.15	0.15	0.15	0.15	1.2	0.3	0.15
3.15	2.85	2.55	2.25	2.25	0.15	0.3	1.95
1.2	0.3	0.6	1.5	0.6	2.25	0.3	0.9
0.15	0.3	0.3	0.6	0.6	0.3	0.9	0.9
3.15	0.9	0.3	0.15	0.3	0.6	0.15	0.6
0.6	0.15	0.6	2.25	0.6	0.6	2.25	0.15
0.6	2.85	0.15	1.2	0.15	0.6	0.3	1.95
0.15	0.3	2.55	0.9	2.25	0.15	0.3	0.9
3.15	0.3	0.3	0.15	0.6	2.25	0.3	0.6
0.3	0.3	1.5	2.25	0.3	0.3	0.3	0.9
0.9	0.6	0.15	1.2	1.2	0.6	0.3	0.15
0.15	0.15	2.55	0.3	0.15	0.3	0.6	1.95
3.15	2.55	0.3	0.6	2.25	0.9	0.15	0.9
0.3	1.8	0.9	0.15	0.6	0.15	1.95	0.6
0.3	0.15	0.6	2.25	0.3	2.25	2.4	0.3
0.6	2.55	0.15	0.9	0.6	0.3	0.15	0.6
0.15	1.2	2.55	1.2	0.6	0.6	1.95	0.15
2.85	0.6	0.3	0.15	0.15	0.3	1.8	1.95

Table 5-1. Continued

0th to 10th	11th to 20th	21st to 30th	31st to 40th	41st to 50th	51st to 60th	61st to 70th	71st to 80th
1.5	0.15	0.6	2.25	2.25	0.3	0.6	0.9
0.15	2.55	0.9	0.9	0.6	0.6	0.15	0.3
2.85	0.9	0.15	0.6	0.3	0.15	1.95	1.2
0.9	0.9	2.55	0.6	0.3	2.25	1.5	0.15
0.6	0.15	0.3	0.15	0.9	0.3	0.9	1.95
0.15	2.55	0.6	2.25	0.15	0.3	0.15	0.9
2.85	0.9	0.3	0.9	2.25	1.5	1.95	0.3
0.6	0.3	0.6	0.3	0.6	0.15	1.5	0.6
0.9	0.6	0.15	0.9	0.3	2.25	0.3	0.6
0.15	0.15	2.55	0.15	0.3	0.3	0.6	0.15
2.85	2.55	0.3	2.25	0.3	0.3	0.15	1.95
0.6	0.6	0.3	0.9	0.6	0.9	1.95	0.9
0.3	1.2	1.2	0.3	0.15	0.6	1.2	0.3
0.6	0.15	0.15	0.3	2.25	0.15	1.2	0.3
		2.55	0.6	0.3	2.25	0.15	0.9
		0.3	0.15	1.8	0.3	1.95	0.15
		0.3	2.25	0.15	0.3	1.2	1.95
		0.6	0.6	2.25	0.6	0.6	0.9
		0.6	1.5	0.3	0.9	0.6	0.3
		0.15	0.15	1.2	0.15	0.15	0.3
		2.55		0.6	2.25	1.95	0.3
		0.3		0.15	0.3	1.2	0.6
		0.3		2.25	0.3	0.3	0.15
		0.3		0.3	0.6	0.9	1.95
		0.9		0.9	0.3	0.15	0.6
		0.15		0.9	0.6		1.8
				0.15	0.15		0.15
					2.25		
					0.3		
					0.3		
					0.3		
					1.2		
					0.15		

V. E. Photolithography Process

The photolithography process for producing a barcode pattern is shown in Fig. 5-3 [14].

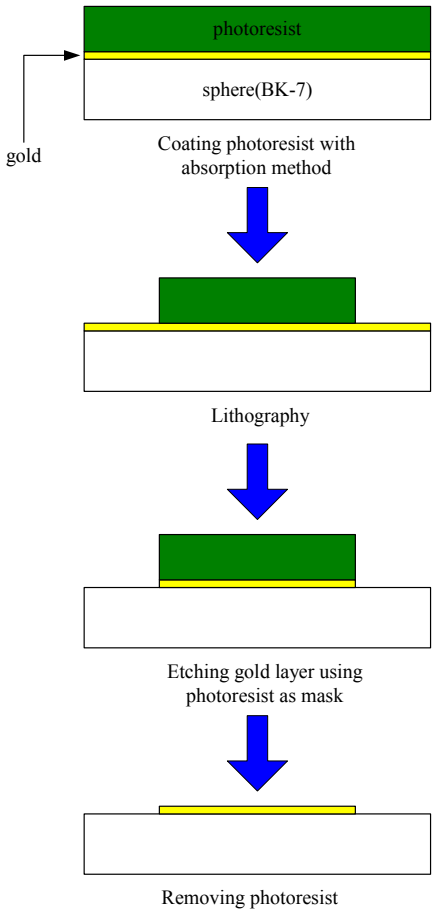

Fig. 5-3. Photolithography process

V. F. Preparation and Application of the Photoresist

A photoresist film of uniform thickness on the surface of a flat substrate is produced using a spin coater. The photoresist thickness can be controlled by adjusting the spin speed. However, this technique is not intended for use with curved surfaces.

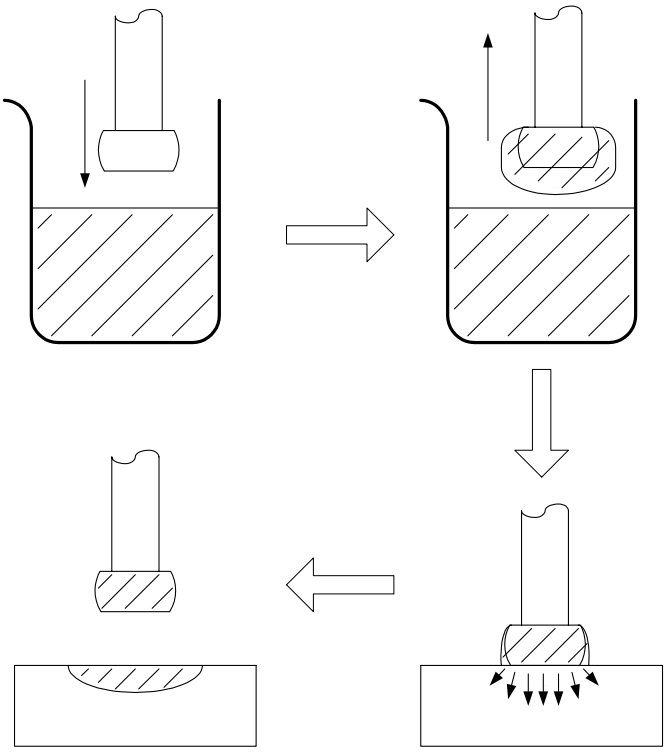

Fig. 5-4. Absorption method

Efforts to apply spin coating to produce a uniform photoresist thickness on an FS surface at various spin speeds and spin accelerating speeds were unsuccessful. Each attempt yielded different thicknesses of photoresist over the surface, which adversely affects the quality of the pattern after exposure and development.

To solve this problem, we used the “absorption method” shown in Fig. 5-4. The sphere is dipped into the photoresist, then removed and placed on an absorbing pad for 2 minutes. The excess photoresist was removed by this method, leaving a uniform coating on the surface of the sphere.

V. G. Photoresist Process Investigations Using Flat Substrates

Shortcomings of the absorption method are that it is not easy to control the photroresist thickness, and the thickness after absorption coating is greater than after spin coating. But thinning of the photoresist to reduce its viscosity makes it possible to reduce the coating thickness. A small amount of pf developer was combined with full strength photoresist in the ratio of 7:1, followed by mixing with a magnetic stirring bar for 24 hours. To compare full strength photoresist with the thinned mixture, 2 gold-coated flat glass substrates were spin coated at speeds of 1000 RPM and 2000 RPM.

The results shown in Fig. 5-5 indicate that for a given spin rate the photoresist thickness is reduced by about 50%. Both full strength photoresist and the mixture were exposed for 10 seconds, developed for 1 minute, and rinsed for 30 seconds. At the center of the samples the photoresist is thicker because at the right focal length photoresist gets more optical energy so that it is less dissolved during development. Based on this result, the 7:1 mixture was selected as coating material for the sphere.

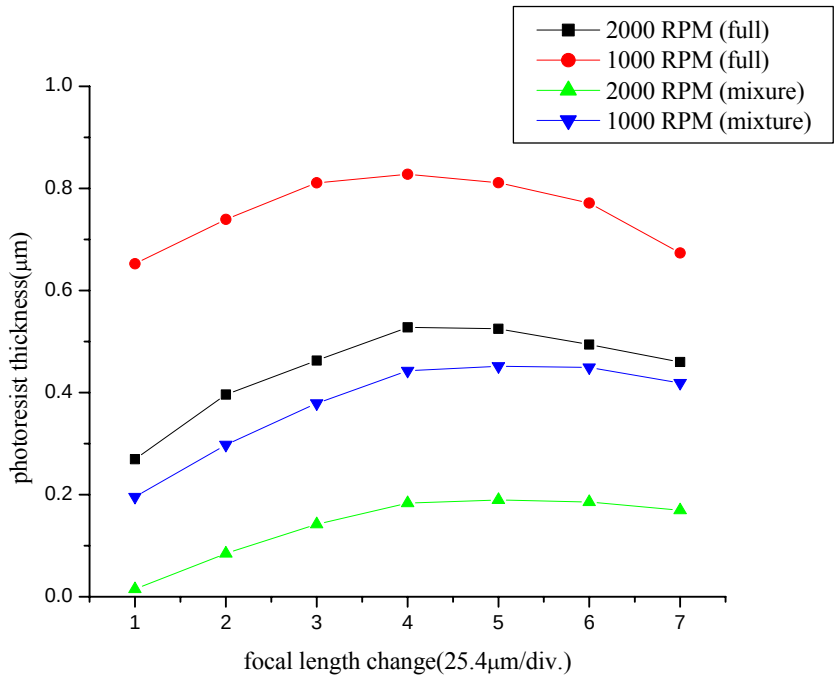

Fig. 5-5. Photoresist thickness after development

When the exposure system is properly focused, the bar pattern is produced accurately with sharp edge definition. If the focal length is not properly adjusted the image on the sphere is blurred, making the bar pattern wider than intended, with poor definition at the edges.

Another important factor is photoresist thickness. Fig. 5-6 and Fig. 5-7 show the effect of spin speed on the thickness and the bar pattern width of the photoresist. The exposure system reduces the mask pattern size by a factor of 10 on the sphere surface at the exact focal length. The bar pattern width of the mask is 140 μm, so the photoresist bar pattern should be 14 μm wide. As indicated in Fig. 5-6, increasing the spin speed from 700 RPM to 2000 RPM reduces the thickness from 0.7 μm to 0.14 μm, while the

data in Fig. 5-7 shows a decrease in bar width from 16.25 μm to 13.75 μm over the same range of spin speeds. Thus, thinner photoresist yields smaller patterns. The data in Fig. 5-7 shows that the pattern size increases with defocusing of the exposure system at 1000 RPM and below, but decreases with defocusing at 2000 RPM. Since the photoresist is thinner at 2000 RPM, less optical energy is needed to completely expose it, so that in the defocused cases even minimally exposed regions were removed easily to leave just very narrow trace of the bars after development.

The data of Figs. 5-6 and 5-7 show that photoresist thickness is critical for getting the desired bar pattern size. It should be thin enough to get the desired bar width and thick enough to be sustained during development. However, it is possible to get the desired pattern dimension with thicker photoresist using longer development times. In such cases the thicker photoresist can sustain a longer development time without being completely removed.

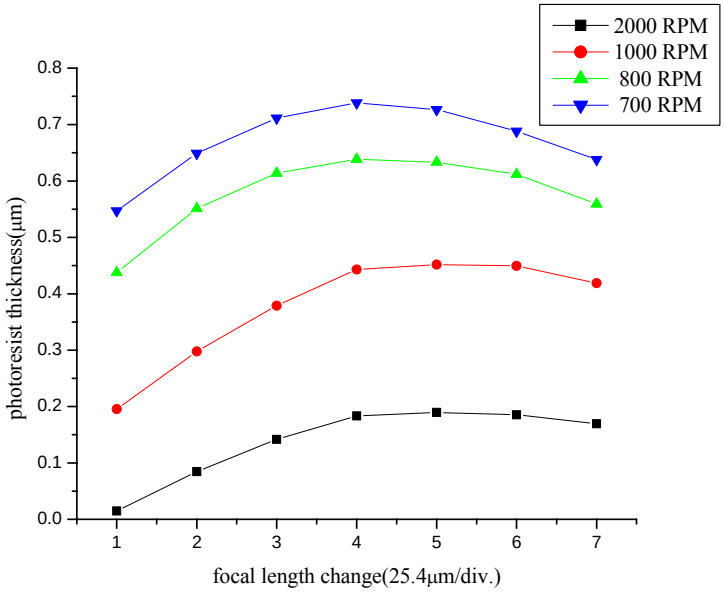

Fig. 5-6. Dependence of photoresist thickness on the spin speed

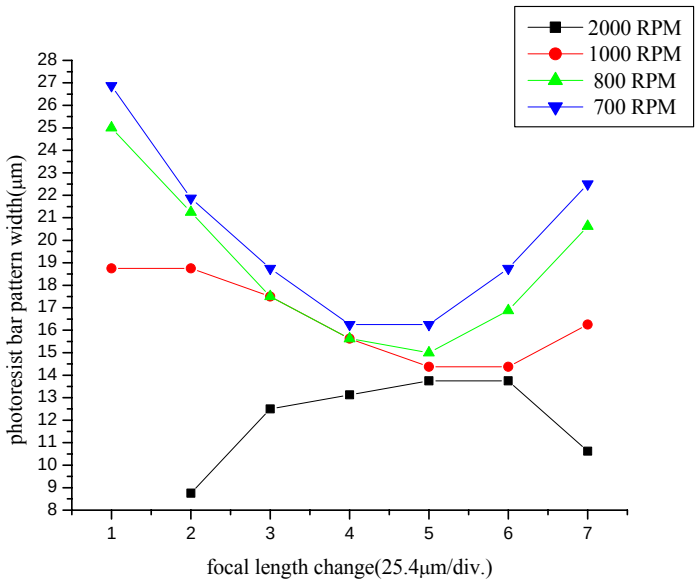

Fig. 5-7. Dependence of photoresist bar pattern width on the spin speed

Photographs of bar test patterns at different spinning speeds and photoresist compositions are given in Fig. 5-8. Each pattern was exposed with same optical energy, varying the focal length by 25.4 μm. At the exact focal length, bar patterns at the edge are clear. But when the exposure system is defocused, the bars are rounded at the ends. It is evident in Fig. 5-8 (a), at the highest spin speed, that only at the exact focal length are good patterns obtained. Away from the exact focal length, the bar patterns have vanish because the thin photoresist has not received enough light energy to be left after development. The other patterns in Fig. 5-8 have sufficient photoresist thickness that the bar patterns have survived after development.

V. H. Exposure of the Spherical Surface

The tests described above (Sec. V. G.) were carried out on a flat surface. When a mask is imaged onto a spherical surface, such that the system is in focus at the equator, defocusing will occur to an increasing extent as the distance from the equator increases. As illustrated in Fig. 5-9, the image plane is displaced from the spherical surface by 15.22 μm for a full angle of the bar pattern of 10º, and 55.85 μm for a full angle of the bar pattern of 20º. The data in Fig. 5-7 shows that the photoresist bar pattern maintains nearly the same width (approximately 1 μm variation) as the system is defocussed by 25 μm, for all of the resist thicknesses (as determined by the spin speed). Thus, the blurring for the 10º pattern should be acceptable. For the 20º case, the blurring will correspond to a total deviation in bar width of 3 μm.

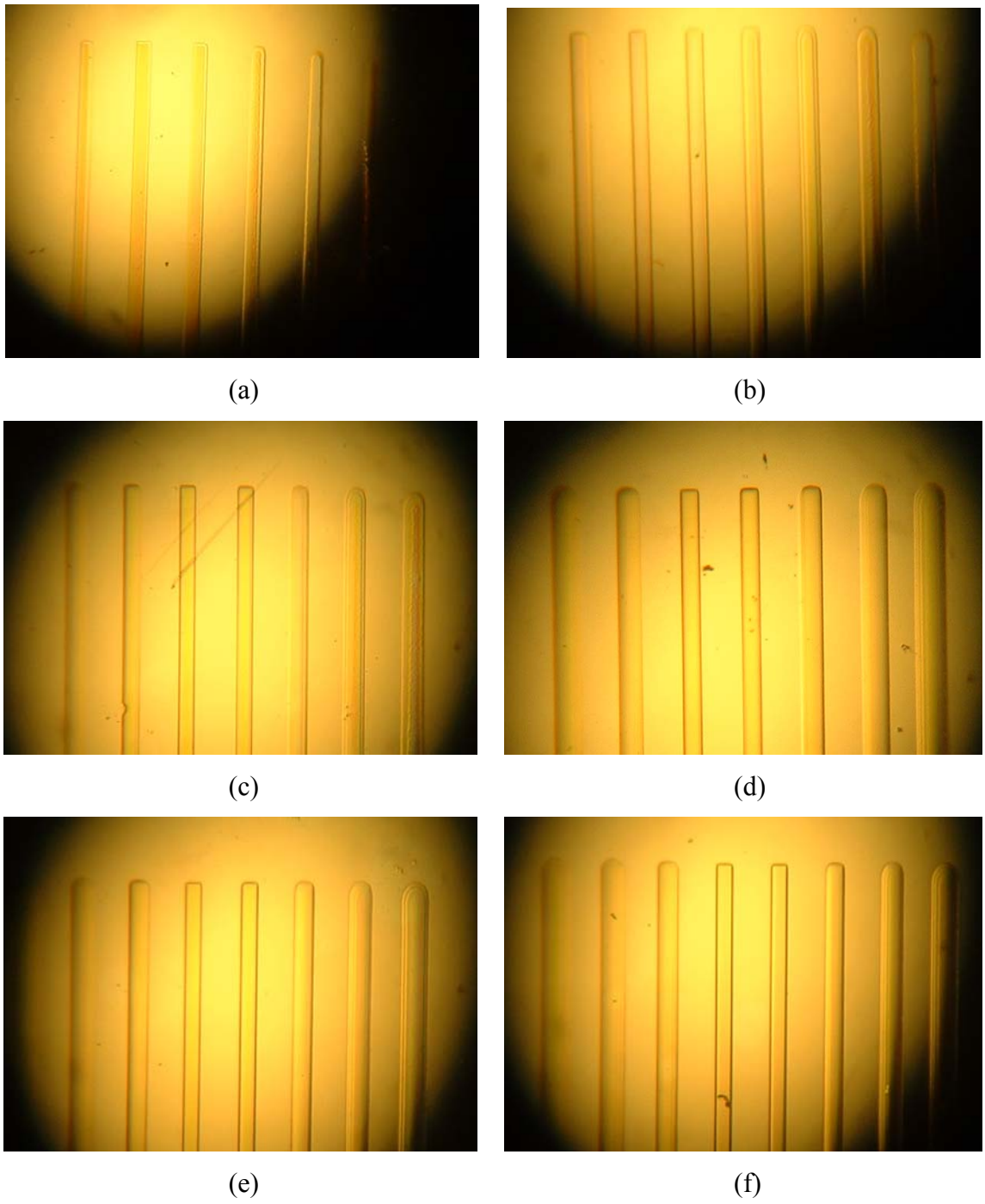

(a) (b)

(c) (d)

(e) (f)

Fig. 5-8. Photos of bar patterns for different spin speeds and photoresist composition : (a) 2000 RPM, full strength, (b) 1000 RPM, full strength, (c) 2000 RPM, 7:1 mixture, (d) 1000 RPM, 7:1 mixture, (e) 800 RPM, 7:1 mixture and (f) 700 RPM, 7:1 mixture

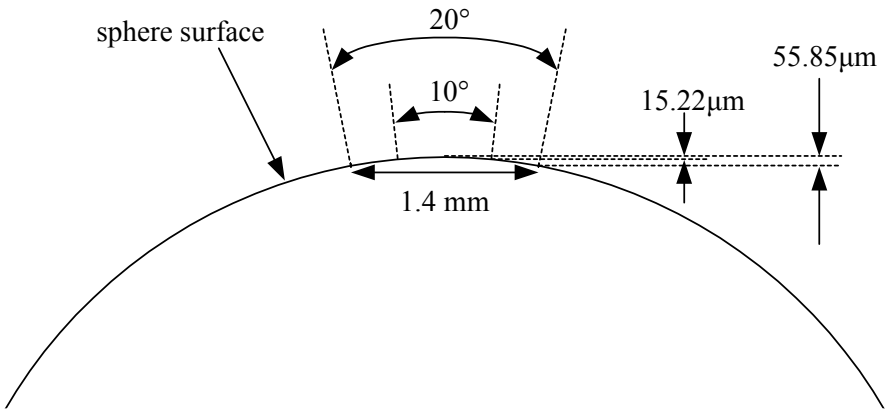

Fig. 5-9. Focal length deviation from the center according to the angle

V. I. Process for Patterning the Spherical Surface

Making a barcode pattern around a sphere is a time consuming job compared with making a pattern on a flat surface. For the case of flat surface the photoresist is developed right after a single shot of light exposure. But the photoresist coated on a sphere by the process described above (Sec. V. A.) is exposed to the air for up to 3 hours while the sphere rotates through 360° twice under computer control. This can have some effect on the photoresist characteristics. And the optimum time for developing and rinsing differs for the two cases even though the light exposure time is same because the photoresist thickness is different for spinning on a flat surface vs. the absorption method applied to a spherical surface.

The photolithography process steps are:

1. Sphere cleaning: sonicating the sphere in acetone and deionized (DI) water
2. Dehydration: removing possible trace of water
3. Photoresist coating, followed by absorption for 2 min.
4. Soft bake: Stabilizing the photoresist for 15 min. at 95 °C
5. Exposure: 35 mJ/cm^2
6. Development/Rinse: 5 min./2 min.
7. Photoresist residue removal with asher: 3 min. at 100 Watt
8. Hard bake: sticking and hardening photoresist for 15 min. at 135 °C
9. Wet etching: 30 sec. for gold layer and 40 sec. for Cr seed layer
10. Photoresist stripping: 15 min. at 95 °C

11. Sphere cleaning: stirring in acetone and DI water

Table 5-2. Measured bar width in 8 separated word patterns sampled from the 80 words distributed around the sphere

word number	7 bit digital word	1 bit bar width in μm
5	0000101	21.25
15	0001111	21.00
25	0011001	21.85
35	0100011	21.25
45	0101110	21.85
55	0110111	20.65
65	1000001	21.50
75	1001011	21.25

After the process, 8 evenly separated bar pattern widths were measured to determine the uniformity of the process around the sphere's circumference.

This is an indication of the ability to coat the sphere evenly around the equator by the absorption method. Ideally the bar width should be 21 μm because the exposure system is designed for 10x reduction from a 210 μm wide mask. As shown in Table 5-2, the maximum bar width is 21.85 μm and minimum bar width is 20.65 μm. With the absorption method, it is difficult to get precisely the same bar width around the sphere equator. However, this is good enough for the compass application, because a 1 μm difference corresponds to an error of less than 0.015°. The total positional error is less than 0.03°, including accumulated error in the angular rotation.

A section of gold barcode pattern on an FS is shown in Fig. 5-10. This section of the pattern contains 2 binary words with bit sequence 1000001 and 1000010. Because of the sphere's curvature, it is difficult to get a photograph in which the entire pattern is in focus. Only at the center of photo is a clean bar pattern captured. Fig. 5-11 is a magnified portion of Fig. 5-10 in which the bar pattern's edge quality is evident. Even though the gold is wet etched, dimensions of the irregularities at the gold bar edges are less than 0.5 μm. This shows that the gold was protected well during etch by the hardened photoresist.

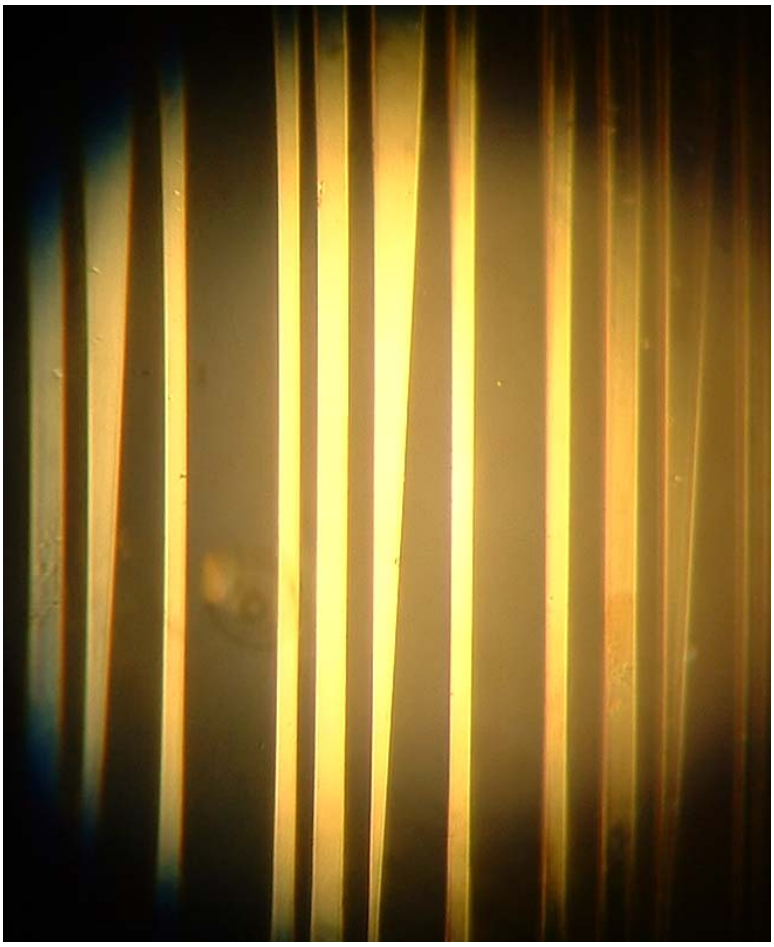

Fig. 5-10. A section of the barcode pattern on a spherical surface of an FS

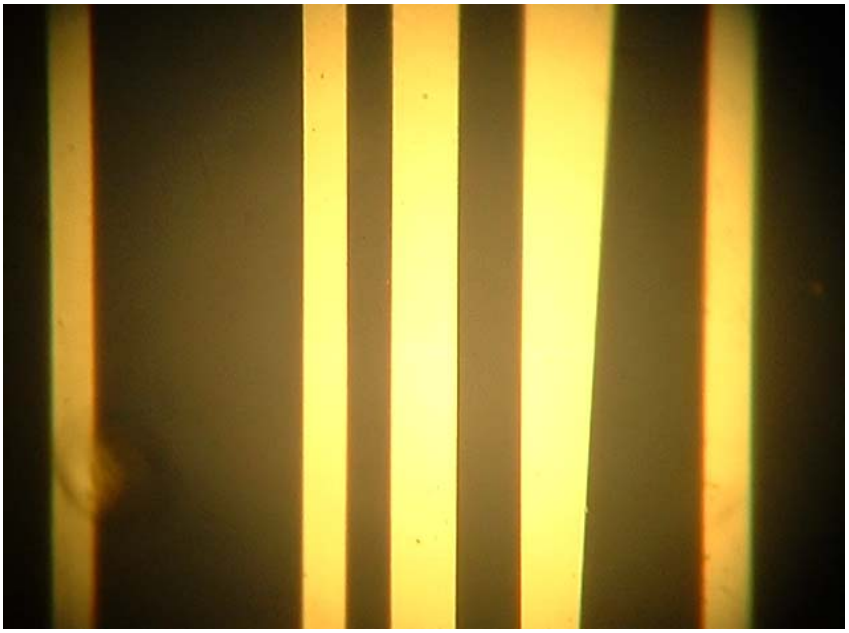

Fig. 5-11. Magnified portion of the photo in Fig. 5-10

As shown in Fig. 5-12, when the sphere is coated by the absorption method the photoresist flows downward. For this reason, the thickness of the photoresist varies with latitude on the sphere, while its thickness is almost independent of latitude. The photoresist thickness decreases from top to bottom. This results in an increase in the bar width from top to bottom, as shown by the photographs in Fig. 5-12. However, more than 90 % of bar length maintains a width of ~ 21 μm.

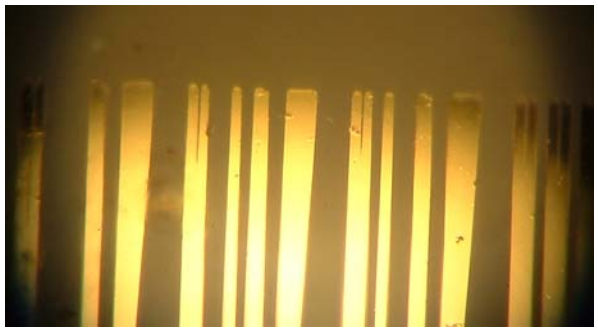

(a)

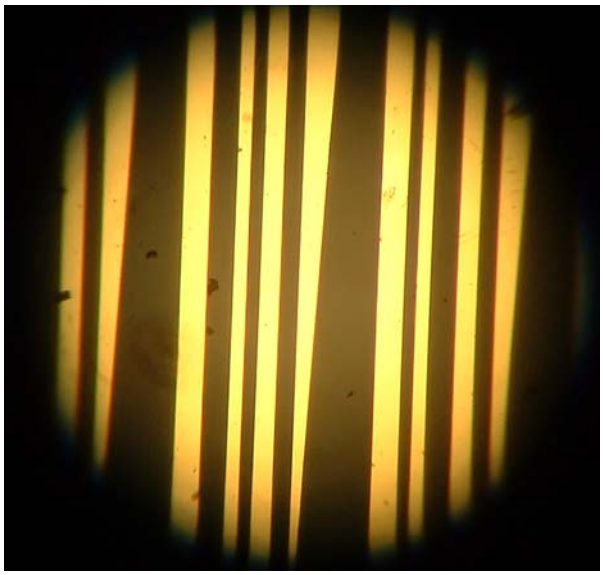

(b)

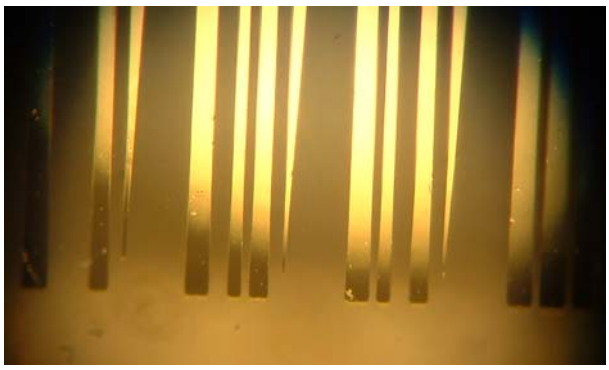

(c)

Fig. 5-12. Bar patterns at different latitudes: (a) top, (b) center and (c) bottom

V. J. Summary of Barcode Pattern Fabrication and Results

Barcode patterns consisting of 80 words containing 15 bit period were produced on gold coated glass spheres with a novel exposure control system featuring a computer-controlled rotation stage and shutter arrangement. In perfecting the fabrication process, the effects of photoresist thickness and defocusing on pattern quality were studied experimentally using a flat substrate. It was found that thinning of the photoresist made it possible to achieve thinner coatings on a flat substrate. Conventional spinning techniques which are widely used to distribute photoresist on flat substrates did not give uniform coverage on the spherical surface. Much better results were obtained by dipping the sphere into photoresist and using an absorption pad to remove the excess. Excellent patterns were obtained on the FSs, with uniform bar widths around the entire 360° periphery of the sphere and an angular error of less than 0.03°, with an 18° latitude scan capability. This result meets the requirements for the fiber optic compass application.

VI. DATA ACQUISITION AND SIGNAL PROCESSING

As the laser is scanned in frequency over the range from 1525 nm to 1565 nm, the light is transmitted to the sensor head via the single mode fiber in the tow cable. In the sensor head, the flying spot moves across the bar code pattern as the laser frequency changes. The light modulated with the bar code scan information and returned to the dry-end SCU via the single mode fiber constitutes the sensor signal. If multiple sensor heads are being monitored, time division multiplexing (TDM) is used to obtain a separate signal from each sensor head. This task is concerned with digitizing the sensor signal and processing it to determine the heading and pitch of one or more sensor heads.

VI. A. Data Acquisition Overview

The bar code pattern consists of 80 words of 15 bit periods each, for a total of 1200 bit periods, physically positioned around the periphery of the FS. A portion of the pattern (typically, about 33 bit periods or slightly more than two words) is read for each scan of the laser. With 6000 samples of the optical signal per scan, 180 samples are collected per bit period. A typical scan is shown in Fig. 6-1. This is the starting point for determining the heading and pitch of the sensor head.

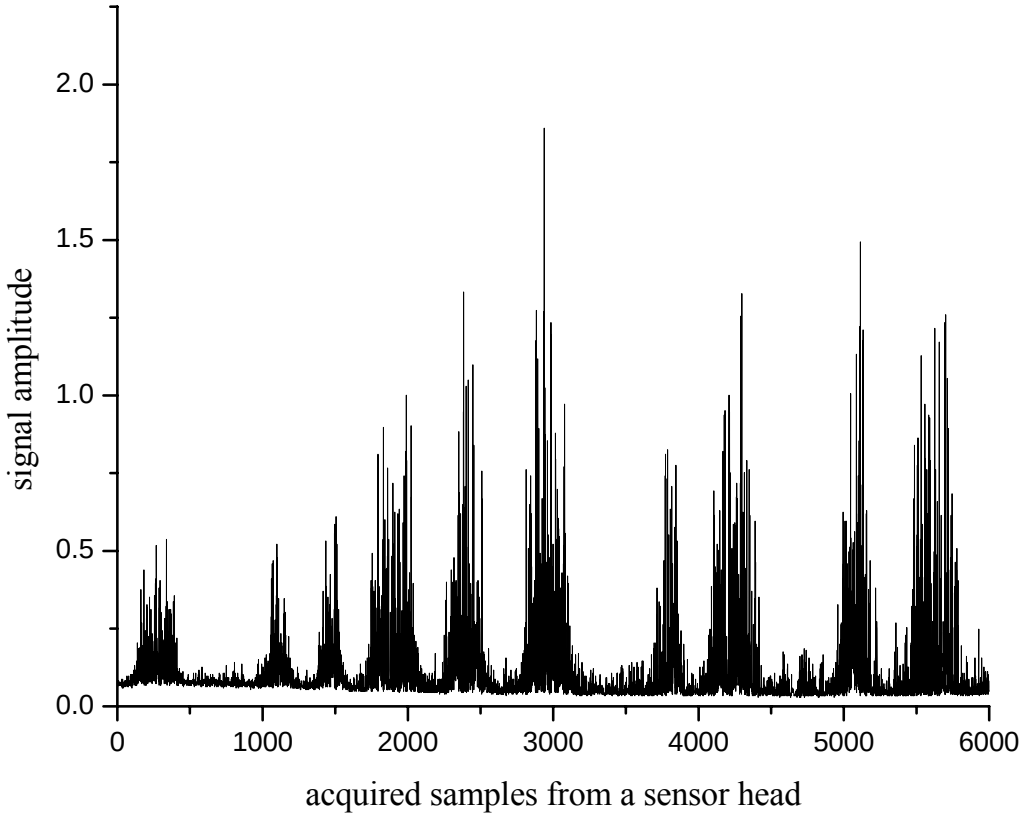

Fig. 6-1. Typical bar code scan

The signal processing algorithm, which has been implemented in LabView, is illustrated schematically in Fig. 6 -2.

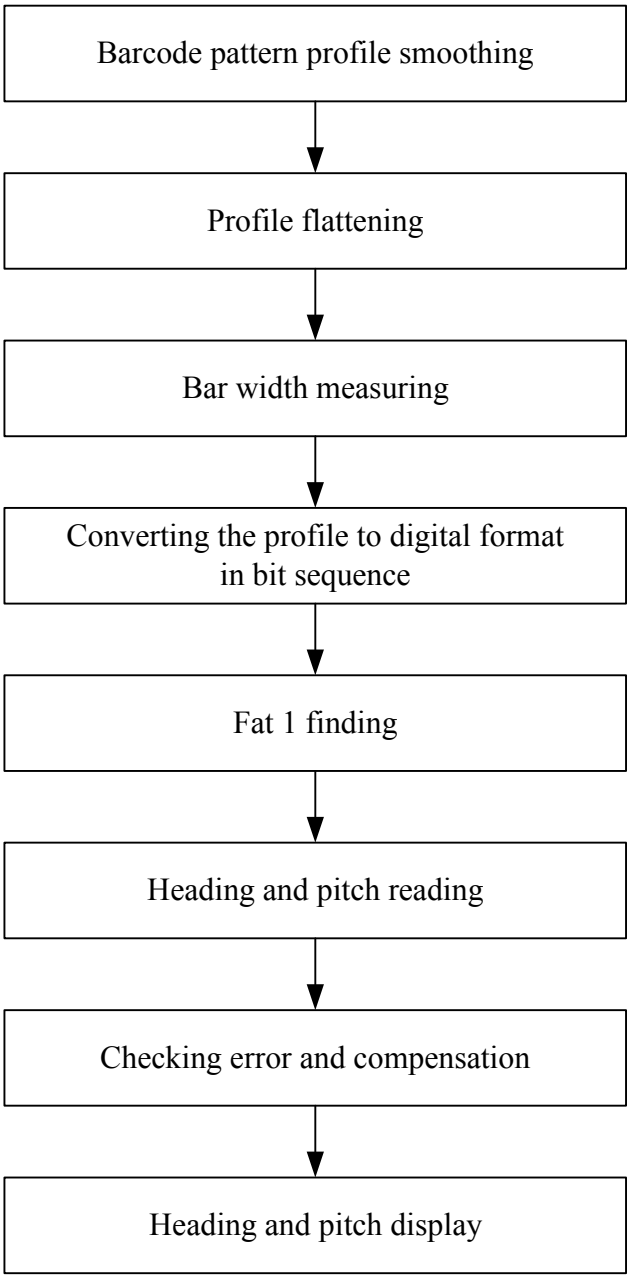

Fig. 6-2. Signal processing for a single sensor head

When multiple sensor heads are monitored with the TDM approach, signals from the individual sensors must be separated prior to the carrying out the signal processing sequence of Fig. 6-2. In that case, the following demultiplexing steps are performed initially:

1. Digitization of the raw TDM optical data - one sample per return pulse
2. Identification of each return pulse with the compass head from which it originated
3. Computation of moving-window average of pulses from each compass head

From this point, the algorithm of Fig. 6-2 is applied independently to the data from each compass head.

VI. B. Barcode Pattern Profile Smoothing

For smoothing the profile, we use the running average method. The sum

$$A_n = \frac{1}{T} \sum_{n=i}^{i+0.5B} S_n , \quad n = i = 0,\ 1,\ 2,\ ....,\ W - 0.5B \tag{6.1}$$

is computed continuously, where A_n is running average value, T is a scale factor, S_n is the raw sample value for the n^{th} sample location, W is total number of samples in the scanning window, and B is the number of samples for 1 bit width. The number of samples included in the sum is 0.5 B. The running average of the data in Fig. 6-1 is given in Fig. 6-3.

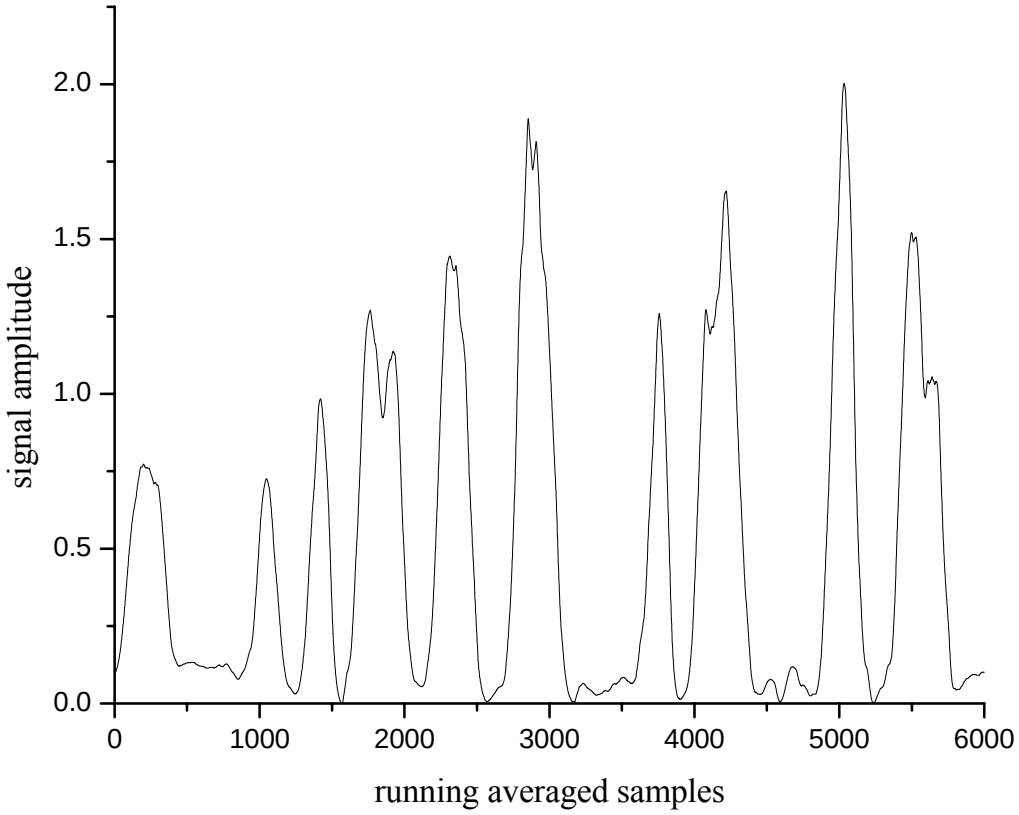

Fig. 6-3. Running average of data in Fig. 6-1

The profile is smoothed without a major increase in the bar width, as shown in Fig. 6-4.

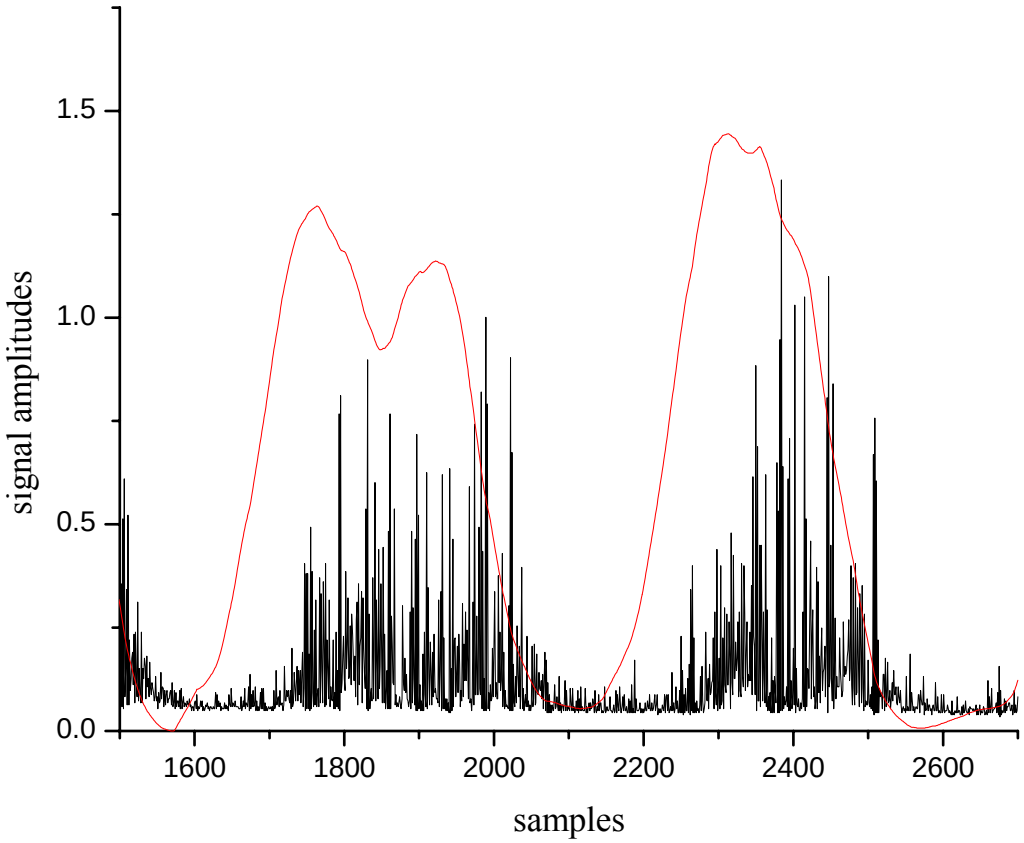

Fig. 6-4. Comparison between raw and running averaged samples, using a portion of the data in Fig. 6-1

To measure the bar widths in the scanning window, we put a fixed reference level and determine the sample locations through which the reference level crossings. 1 bar width is determined by the number of samples between 2 consecutive reference level crossings, one of which is from the rising slope and the other from the falling slope of a bar. If the raw sample profile is not smoothed by using a running average, there will

generally be several reference level crossings for each bar due to the noisy nature of the raw data. By smoothing, we can obtain only two reference level crossings per bar.

VI. C. Normalization of Scan Data

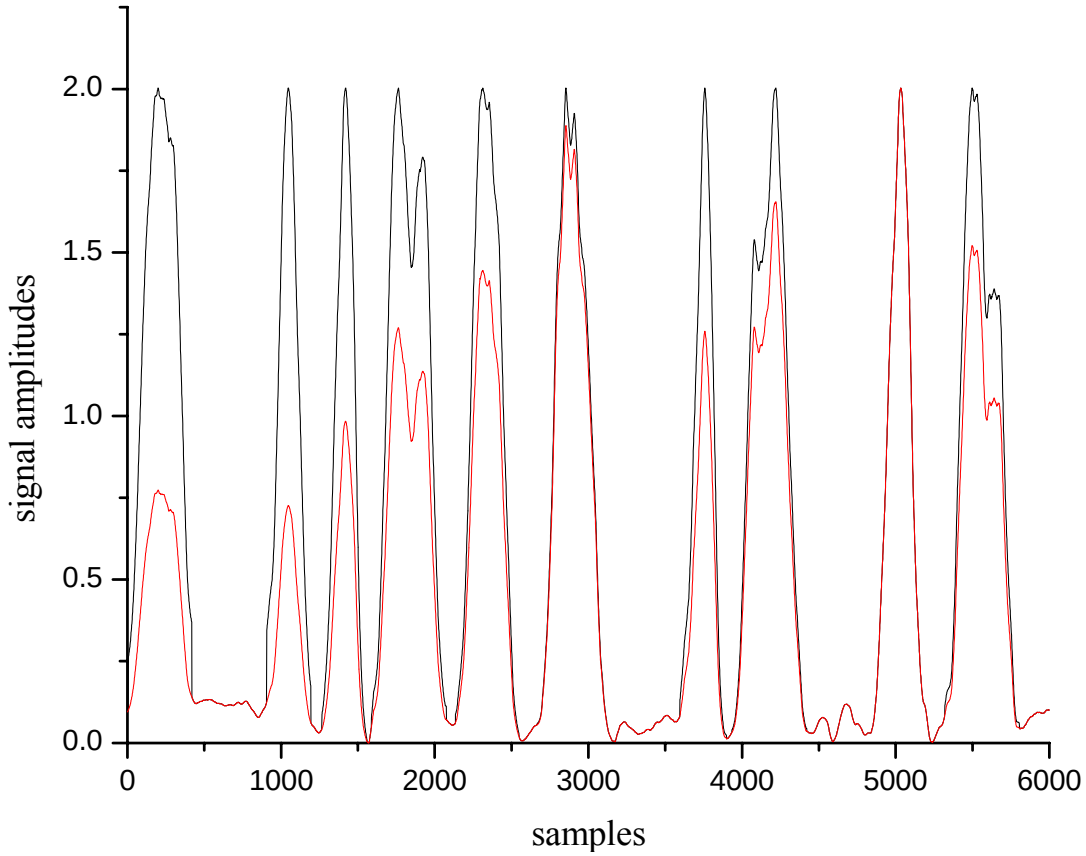

Fig. 6-5. Normalization of the scan pattern, with peaks adjusted to the same height

To obtain equal bar widths even though the peak heights vary, the smoothed scan pattern was normalized such that the height of each peak was the same, as in Fig. 6-5. Each signal value between two nulls was multiplied the common factor required to make

the peak height the same as all the other peaks. From multiple measurements, it was found that ~ 30 % of the height of the peak for each bar is the optimized level for determining the actual bar widths. Fig. 6-6 shows that the bar width at 30 % of the peak before and after flattening maintains almost same.

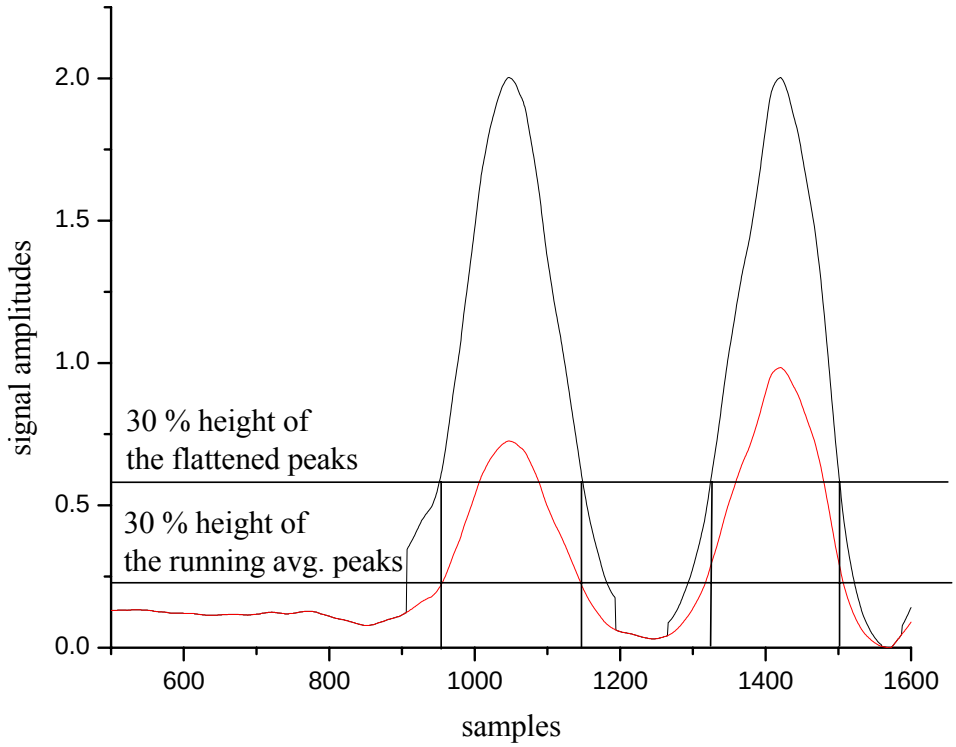

Fig. 6-6. Bar widths at 30 % of signal peak, before and after normalization

VI. D. Measurement of Bar Widths and Conversion to a Digital Format

The bar widths are measured from the normalized scan profile. The bar width is defined as the number of samples between two consecutive reference level crossings - one at the rising slope sample point (RP) and the other at the falling slope sample point (FP). Each bar has an RP - FP pair, so there are as many RP-FP pairs as bars. By

measuring the spacing, in number of samples, between an RP and the next FP, we can determine the number of bit periods contained in a bar.

Each word in the bar code pattern contains 3 types of bars: the "one" bit, fat "one" bit, and "analog" bar. The RPs (but not the FPs) are separated by an integral number of bit periods. Thus, by measuring the spacing between consecutive RPs, we can know how many bit periods are included. After counting the total number of bit periods between the RPs, the widths of the bars are determined from the spacing between consecutive RPs and FPs. Because the number of samples 1 bit period is 180, the RP-FP and RP-RP spacings are divided by 180 to count the number of bit periods. The quotient is rounded off to the nearest integer to determine the number of bit periods. This is an integer, except for two cases: the width of a "fat one" is 1.5 bit periods, and the width of an analog bar lies in the range from 0 to 3 bit periods, depending on the pitch of the compass head. Table 6-1 shows the RP and FP locations from the smoothed and normalized scan data of Fig. 6-5. The corresponding number of bit periods in each bar, equal to the RP-FP separation divided by 180, is also given in that Table. The RP-RP separations from the data of Table 6-1 are given Table 6-2. Table 6-2 shows that consecutive RPs are separated by close to an integral number of bit periods.

Table 6-2. RP-FP pairs and bit numbers in each bar

RP-FP sample location pairs										
RP	57	957	1327	1655	2207	2751	3666	4011	4916	5391
FP	359	1143	1508	2006	2476	3056	3833	4319	5125	5725
Each bar width and 1 bit number in each bar										
Bar width	1.68	1.01	1.1	1.91	1.48	1.67	0.97	1.7	1.32	2.11

Table 6-2. RP-RP pairs and bit numbers in each bar

RP-RP width	5	2.06	1.82	3.07	3.02	5.08	1.92	5.03	2.64
Bit number	5	2	2	3	3	5	2	5	3

The results of Table 6-1 and Table 6-2 are combined to produce a digital bit sequence of the scan in Table 6-3. The total number of bit periods is 32, which equals slightly more than two 15-bit words.

Table 6-3. Total digital bit sequence from the first RP to the last FP

1	1	0	0	0	1	0	1	0	1	1	0	1	0	0	1	1	0	0	0	1	0	1	1	0	0	0	1	0	0	1	1

One factor which must be taken into account is that the scanning window does not always starting with an RP and finish with a FP. There are four cases of RP and FP sequences, shown in Fig. 6-7.

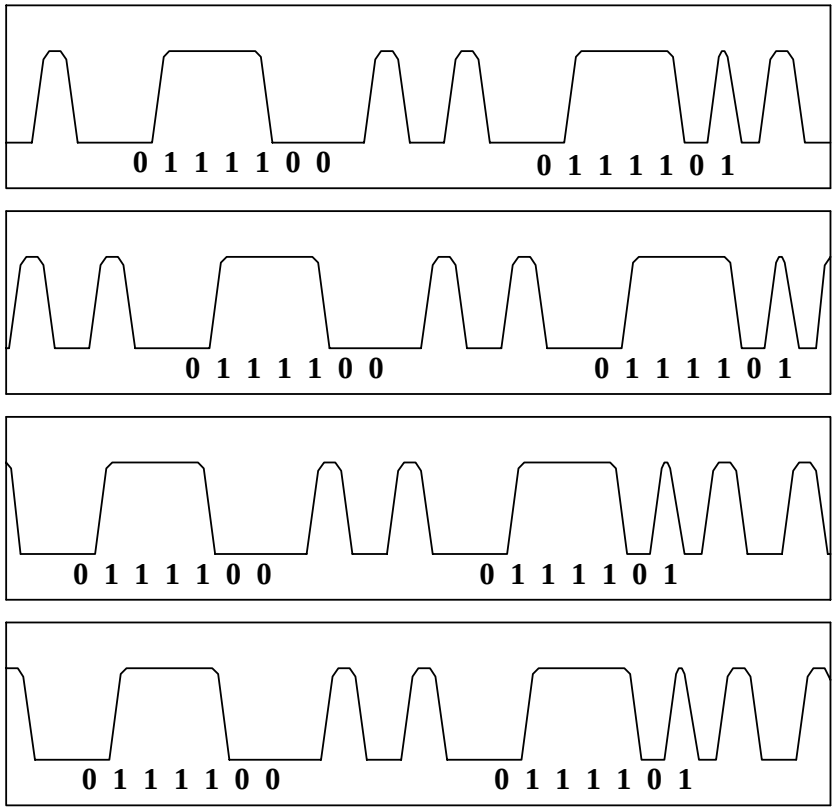

Fig. 6-7. Four cases of RP and FP sequence

All four cases have the same consecutive seven-bit words 0111100 and 0111101. The first scan starts with an RP and finishes with a FP, the second starts and finishes with an RP, the third starts and finishes with an FP, and the last starts with a FP and finishes with an RP. We need to take into account which of the four cases applies when we convert the profile to the digital format. Spacing from window starting sample point and first RP or FP is measured, divided with sample for 1 bit (= 180) and the quotient is rounded off to 0 or 1 bit period. Then we can get the complete bit sequence of the scan.

With this method, the bit sequence of Table 6-3 is modified by the addition of a single "0" bit at the end of the sequence.

VI. E. Locating the "Fat One"

The 15 bit periods of one word are composed of a fat "one" bar 1.5 bit periods wide, a fat zero 1.5 bit periods wide, an analog bar occupying 3 bit periods, a null 1 bit period wide, a binary pattern 7 bit periods wide, and a null 1 bit period wide. Once the "fat one" is located, we can easily find the analog section and the 7 digital bits. Four criteria are used to locate the "fat one":

1. The "fat one" bar width should be in the range of ~1.5 bit periods (eg.: 1.2 < fat one < 1.8)
2. The RP-RP spacing between the fat 1 bar and analog bar should be 3 bit width.
3. The next bar width past the "fat one", the analog bar width, should be less than 3 bit periods.
4. The RP-RP spacing between the analog bar and the next bar past the analog bar should be greater than 4 bit widths.

Applying these conditions, the fifth bar in Fig. 6-5 is the "fat one" bar. The next bar past the "fat one" bar is analog bar, the next is a null, and the binary pattern occupies the next 7 bit periods. The entire bit sequence is shown in Fig. 6-8.

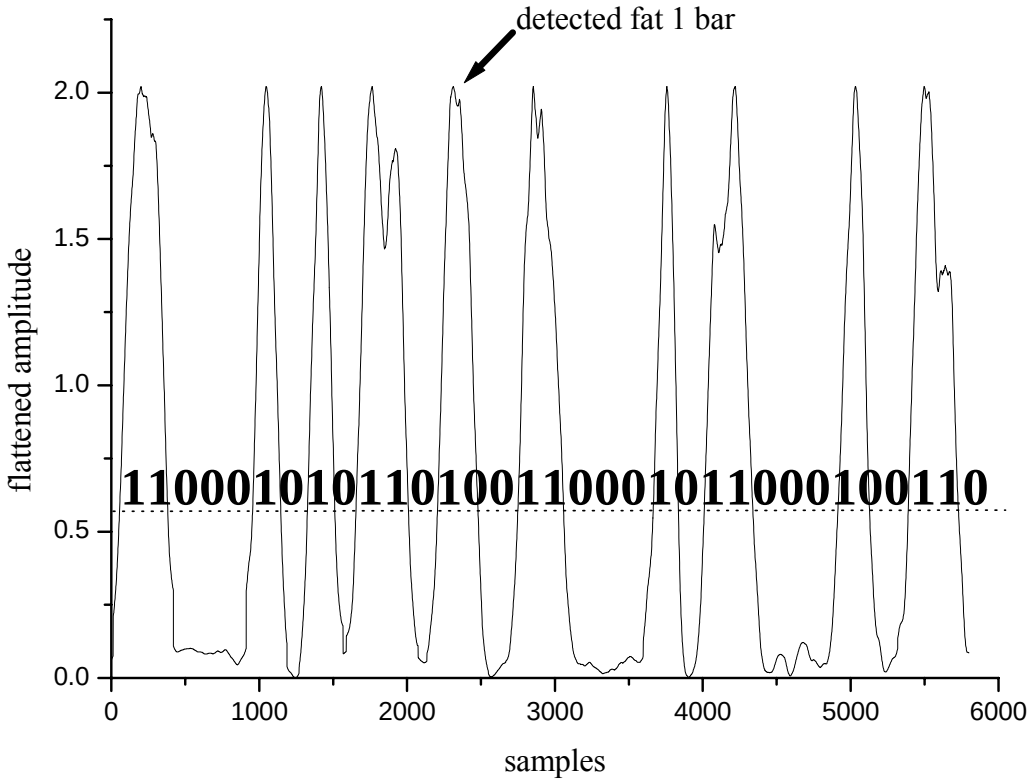

Fig. 6-8. Digital conversion of barcode scan pattern

VI. F. Heading and Pitch Reading

After the "fat one" has been located, the 7 digital bits are read for coarse heading determination. If there are less than 17 bits before the "fat one" bar, the 7 digital bits after the "fat one" are read. Otherwise, the 7 digital bits ahead of the "fat one" are read for heading. In Fig. 6-8, we read 7 digital bits of 0101100 following the "fat one", "fat zero", analog pattern, and null bit period. 0101100 is a binary "44", the 44^{th} of 80 words. Because 1 word corresponds to 4.5° in angle, 0101100 corresponds to 44*4.5 = 198° relative to the start of the pattern. By measuring the number of samples between the

starting point of the scan and the RP corresponding to the “fat one”, we can read the heading much more precisely.

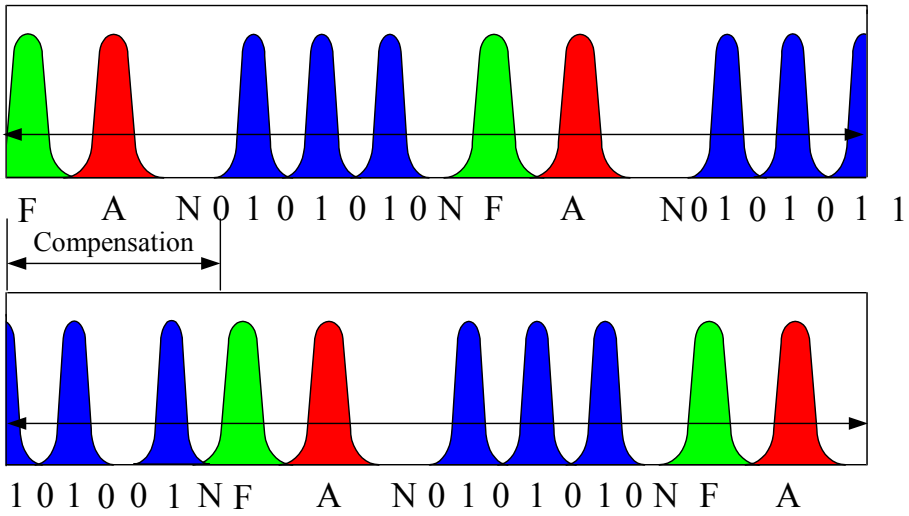

Fig. 6-9. Precision reading scheme for heading

Fig. 6-9 illustrates the principle of obtaining a precise heading measurement. Both scans illustrated contain the 7 digital bits 0101010. We assume that the heading is exactly read by the binary code when the RP of the “fat one” starts at the first sample point of the scanning window. When the RP of the “fat one” bar doesn’t start at the first sample point, we use the sample number of the RP of the “fat one” bar to correct the binary value for fine resolution. Since one bit period is composed of 180 sample points, the resolution is 0.3°/180 = 0.00167°. 7 digital bits of 0101010 in Fig. 6-9 read 198°. If the number of samples between the starting point of the scan and the RP of the “fat one” bar is 1130, then the compensated reading is 198° + 0.00167°*1130 = 199.8871°.

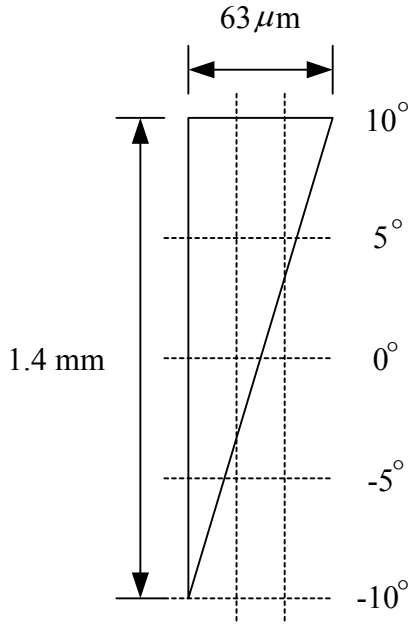

Fig. 6-10. Pitch according to analog bar width

The pitch is measured by determining the analog bar width (spacing between RP and FP), as shown in Fig. 6-10. Three bit periods are allocated to the analog section of the pattern, corresponding to 180*3 = 540 sample points. Thus, 270 samples equal 10° in pitch, and 1 bit period equals 20°/3 = 6.6667°. At the center of analog bar, the pitch is zero. From Table 6-1, the analog bar width is 1.67 bit period, so the pitch is (1.67-1.5)*6.6667° = 1.1333°.

In calculating the heading and pitch, we can increase the resolution by increasing the number of samples per scan. Ultimately, the noise in the scan (Fig. 6-1) will limit heading and pitch resolution.

VI. G. Error Compensation

We can assume that in the towed array application, the sensor head will rarely change its direction suddenly. So a big jump of the heading value (e. g., 30°) can be considered an error. The signal processing program stores the most recent heading and pitch values, and compares the current heading and pitch values with the stored ones. If there is a big difference between the previous value and the current one, then we ignore the current one and replace it with the previous one. We express H_n as the current heading value, H_{n-1} as the previous heading value, P_n as the current pitch value, P_{n-1} as the previous pitch value. The "fat one" bars are found first, to get the location of the "analog bars" and the 7 digital bit sequences. The program first checks the sample numbers of the RPs of the "fat ones". There are 3 cases: no "fat one", one "fat one", and two "fat ones" (in this case, there are two heading values of H_n and H_n'). In the case of no "fat one" bar, an absolute error is declared. Even though at least one "fat one" bar is found, it is necessary to check to see if it is the right one. If it is determined to be the right one, then there is no need for error compensation. Otherwise, error compensation should be done, as in Fig. 6-11.

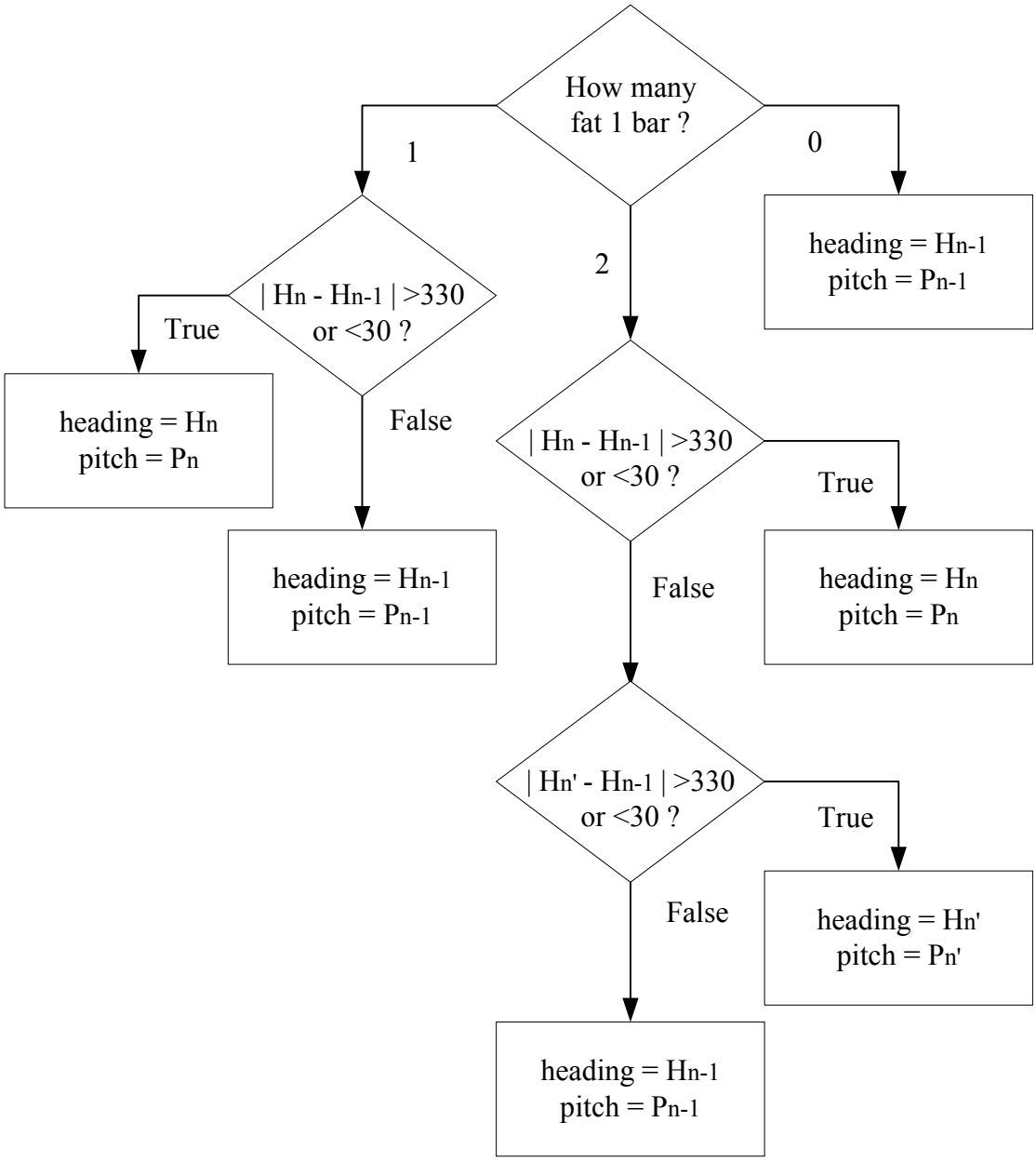

Fig. 6-11. Error compensation flow chart using the location of the RP of the "fat one" bar

Checking and compensation is performed for each bar code pattern scan, as in Fig. 6-11. With this compensation algorithm, we can suppress undesired heading jumps. For no "fat one" bar, we just retrieve the previous heading and pitch values. For one "fat one" bar, we subtract H_{n-1} from H_n and take the absolute value to determine if a jump has occurred. If a jump has occurred, we retrieve the previous values; otherwise, we take the current values. For two "fat one" bars, we check with H_n to see if a jump has occurred. If there is no jump, then we use H_n and P_n as heading and pitch values. If a jump is indicated with H_n, we use H_n' for checking for a jump. If we don't get the right heading value with either H_n or H_n', we retrieve H_{n-1} and P_{n-1} as the heading and pitch values.

VI. H. Signal Processing for Time Division Multiplexing (TDM) with Multiple Compasses in the Array

The previous discussion in Section VI. A. through Section VI. G. is concerned with the processing of data for a single compass head. When multiple compasses are distributed along the array cable, time division multiplexing (TDM) is used to separate the signals from the individual compass heads. The TDM arrangement is illustrated in Fig. 6-12.

Pulses of light from the swept-frequency laser are gated by an integrated optical modulator into the fiber which carries light to and from the sensor heads. Return pulse amplitudes are digitized and processed separately to obtain the heading and pitch for each compass head using the algorithms described above for a single compass head. The reflected pulses from the sensor heads follow the optical modulation pulses after a time spacing determined by the physical time delay of light propagating in the fiber. If the fiber length between the dry-end SCU and first sensor head is N m, then the round trip propagating time, T, of light can calculated by

$$T = \frac{2N}{c} n \ \text{[sec.]} \qquad (6.1)$$

where $c = 2.998 \times 10^8 [m/\text{sec}]$ is the light speed in the air and n = 1.4535 is the refractive index of the fiber core. With a fiber length of 150 m, T is 1.4535 μs. Because the DAQ card takes 5 samples per μs, the leading edge of the first reflected pulse follows 7 or 8 samples behind the modulation pulse.

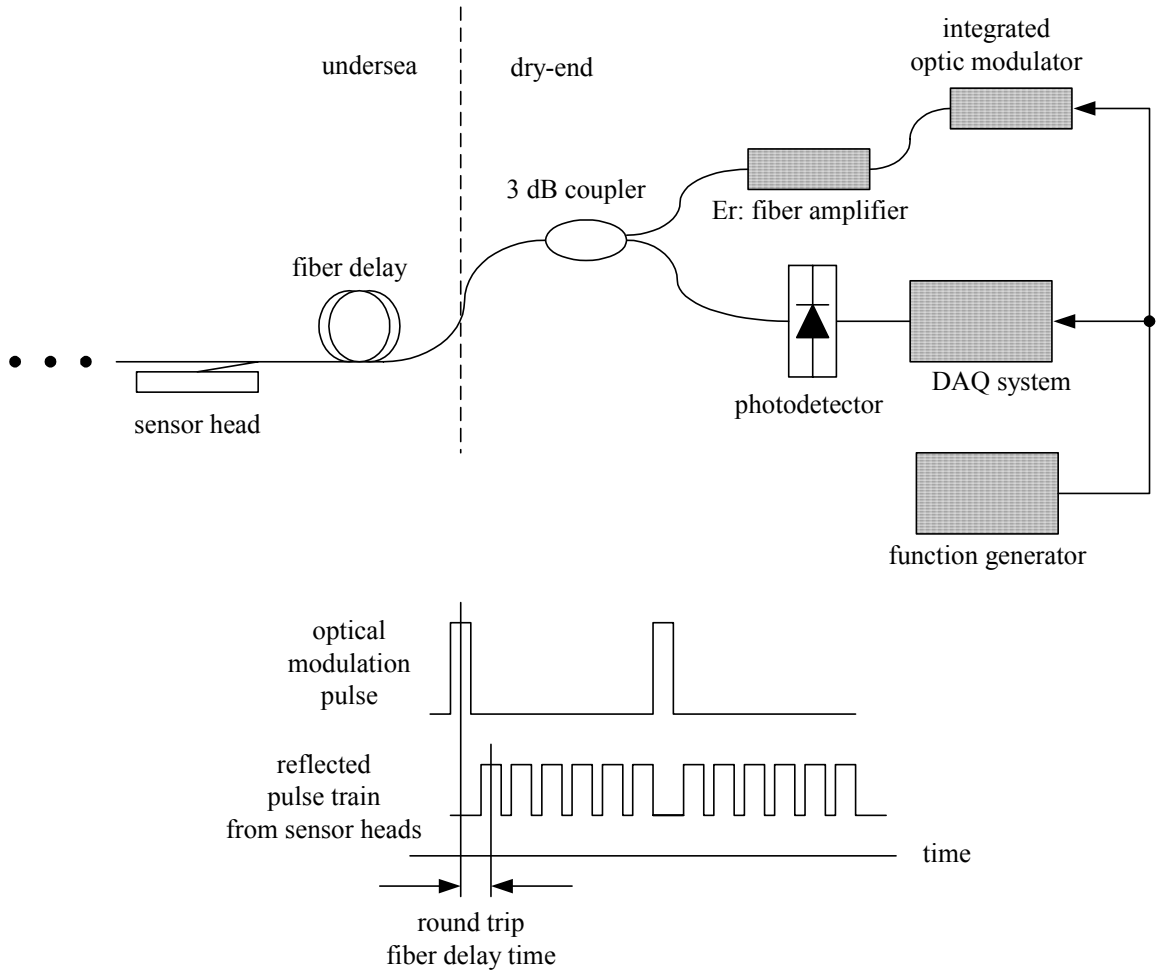

Fig. 6-12. Pulse trains from the optical modulator and or heads

VI. I. Synchronization of Optical Modulator and Data Acquisition (DAQ) System for TDM

When two function generators operated asynchronously were used as clocks for the optical modulator and the DAQ system, timing mismatch problems led to errors in digitization of the TDM data. Fig. 6-13 illustrates the effect of timing mismatch between the function generator and the DAQ system.

A train of square pulses generated by a function generator enters the DAQ system which digitally samples the input data and displays the input data signal. For short time measurement, internal clock mismatch between two instruments, e. g., the oscilloscope and the function generator, is not a serious problem. But for our application, internal clock match is absolutely required because we are acquiring the all the sample points throughout each scan. The sampling times of the DAQ system should always fall in the incoming pulse duty cycle. We generated a 500 kHz square wave with ± 0.1 V amplitudes with an HP function generator and acquired the data with a National Instrument PCI-6110 DAQ card with a 100KS/s sampling rate.

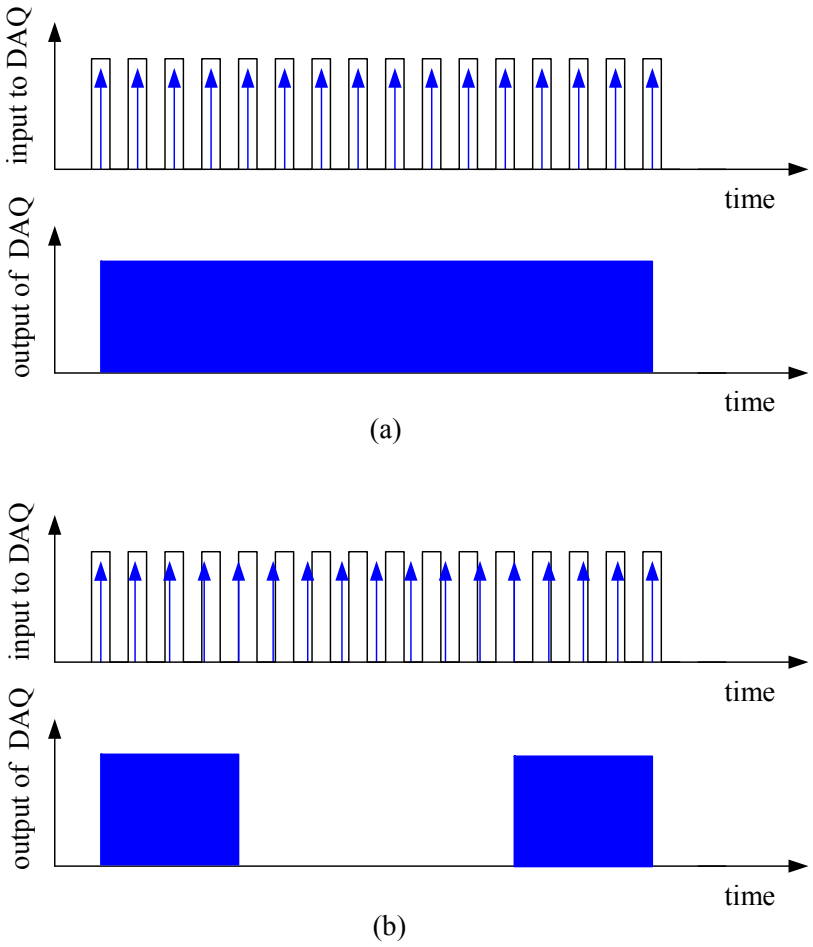

Fig. 6-13. Comparison of the cases between internal clock speeds (a) match and (b) mismatch

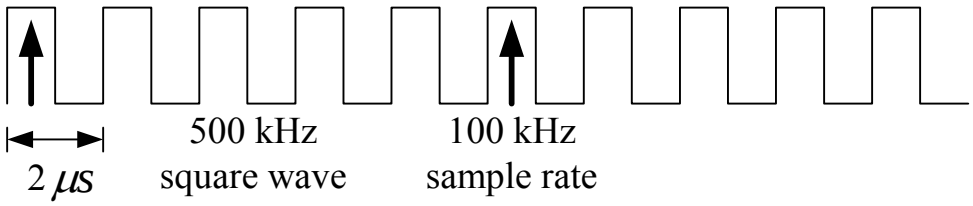

Fig. 6-14. Function generation and sampling

If the clock speeds were same, the DAQ output should have been like Fig. 6-13 (a) because the PCI-6110 DAQ card gets 1 sample from 5 pulses from the function generator, as in Fig. 6-14, and therefore the DAQ cannot distinguish the pulse change. But the DAQ output is shown in Fig. 6-15. The result of Fig. 6-15 confirms that there is a deviation of 8 μs in synchronization between the function generator and the DAQ system time during an elapsed time of 1 sec. The RC time constant of the DAQ card causes the rising and falling edges of the data pulses.

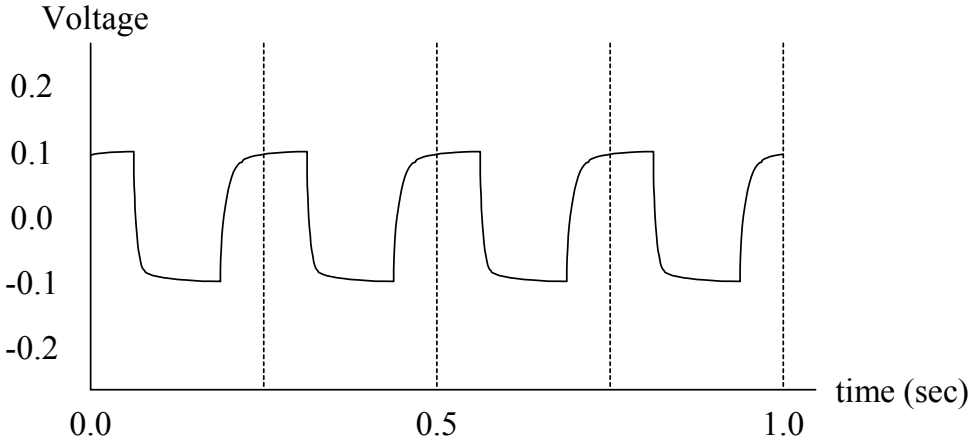

Fig. 6-15. DAQ output after data acquisition of 500 kHz square wave

The DAQ card reads the correct voltage input for a 0.125 sec time period because sampling time occurs during the data pulse and misses the correct voltage input during next 0.125 sec time period because the sampling time occurs between data pulses. The DAQ output alternates between pulse and no pulse with a time period of 0.125 sec.

A solution for avoiding this internal clock mismatch is to use the signal pulses for synchronization, rather than each instrument's internal clock. This method is implemented in software with a Labview program. We make use of the known delays between the optical modulation pulse and the reflected pulses from the sensor heads. Internal clock mismatch is not a factor if we use the signal pulses themselves for matching the signals.

A 100 kHz, 10 % duty cycle square wave from the HP function generator serves as the clock input to both the optical modulator and the DAQ system, as illustrated in Fig. 6-16. The TDM sensor data is acquired with a National Instrument PCI-6110 DAQ card at 5 M samples/sec. Thus, the DAQ card takes 5 samples during the 1 μs duration of a data pulse. DAQ system begins to collect the sample values from 2 channels.

DAQ system stacks the sample values in the memory from 2 channels in parallel at one sampling time. To the first channel enter the electrical pulses which are generated from function generator for the optical modulator. To the second channel enter electrical pulses reflected from the sensor heads.

The DAQ system acquires optical modulation pulse during the initial period when the internal clocks are well-synchronized, detects the sample at the pulse center, and records the sample location. Subsequently, we make use of the knowledge that the first reflected sensor pulse follows 7 or 8 sample periods after the modulation pulse. By repeating this process throughout the mirror scanning time, the clock mismatch problem illustrated in Fig. 6-13 (b) is eliminated.

Demultiplexing of the TDM data is achieved by counting the number of samples between the sensor data pulses. The sensor heads in the array are separated by 150 m of fiber, so the corresponding pulses are separated by 7 or 8 sample pulse times, as illustrated in Fig. 6-16 for the case of 2 sensor heads.

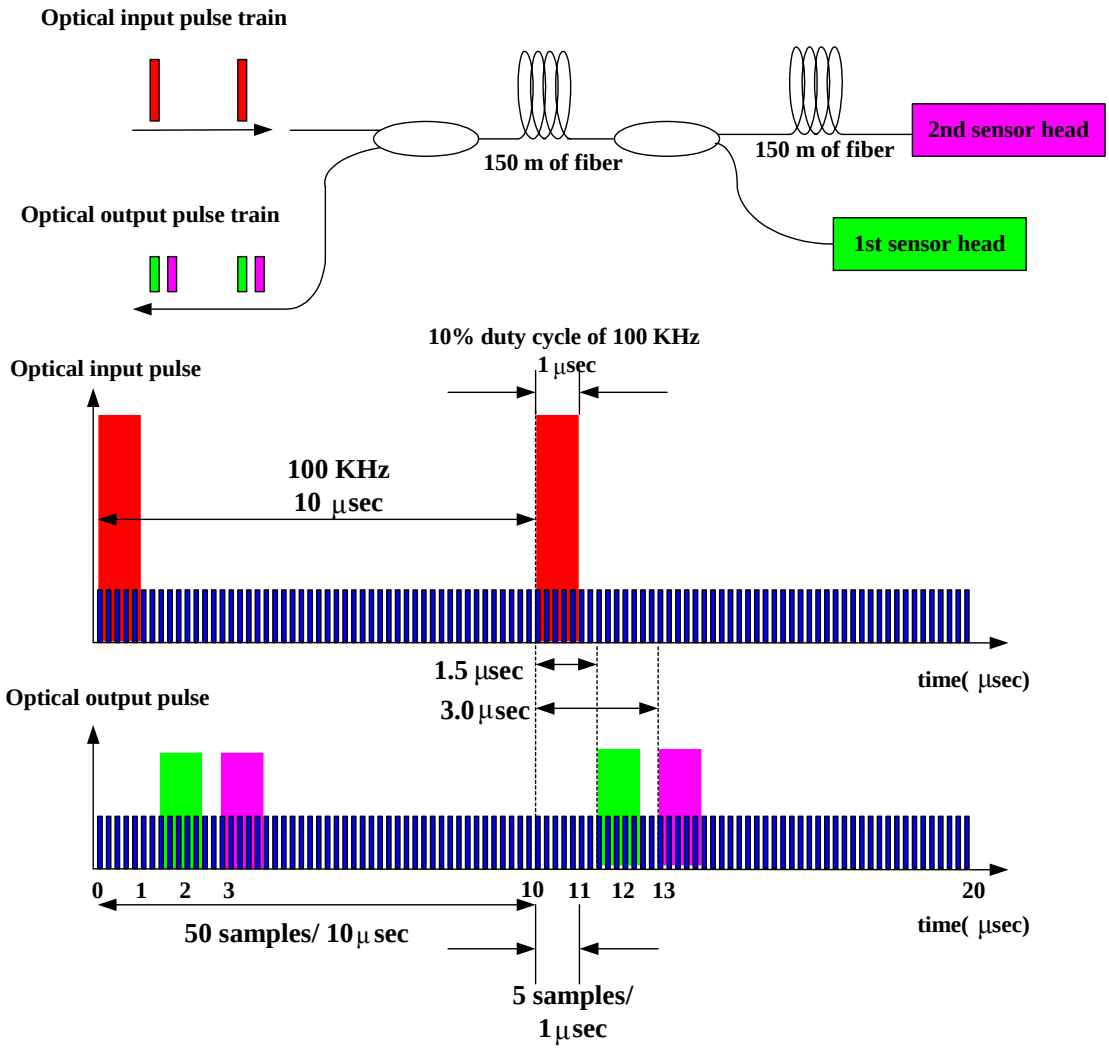

Fig. 6-16. Sample timing diagram using 2 sensor heads

VI. J. DAQ with NI PCI-6110

We don't have to acquire and process samples at the 5 MS/s rate of the DAQ system for sensor reading. Because less than 200 samples are enough for reading a single bit, we can select sparsely distributed samples. A sample selection scheme to get 60

samples for 1 bit period is illustrated in Fig. 6-17, when we used 2 sensor heads separated by 150 m.

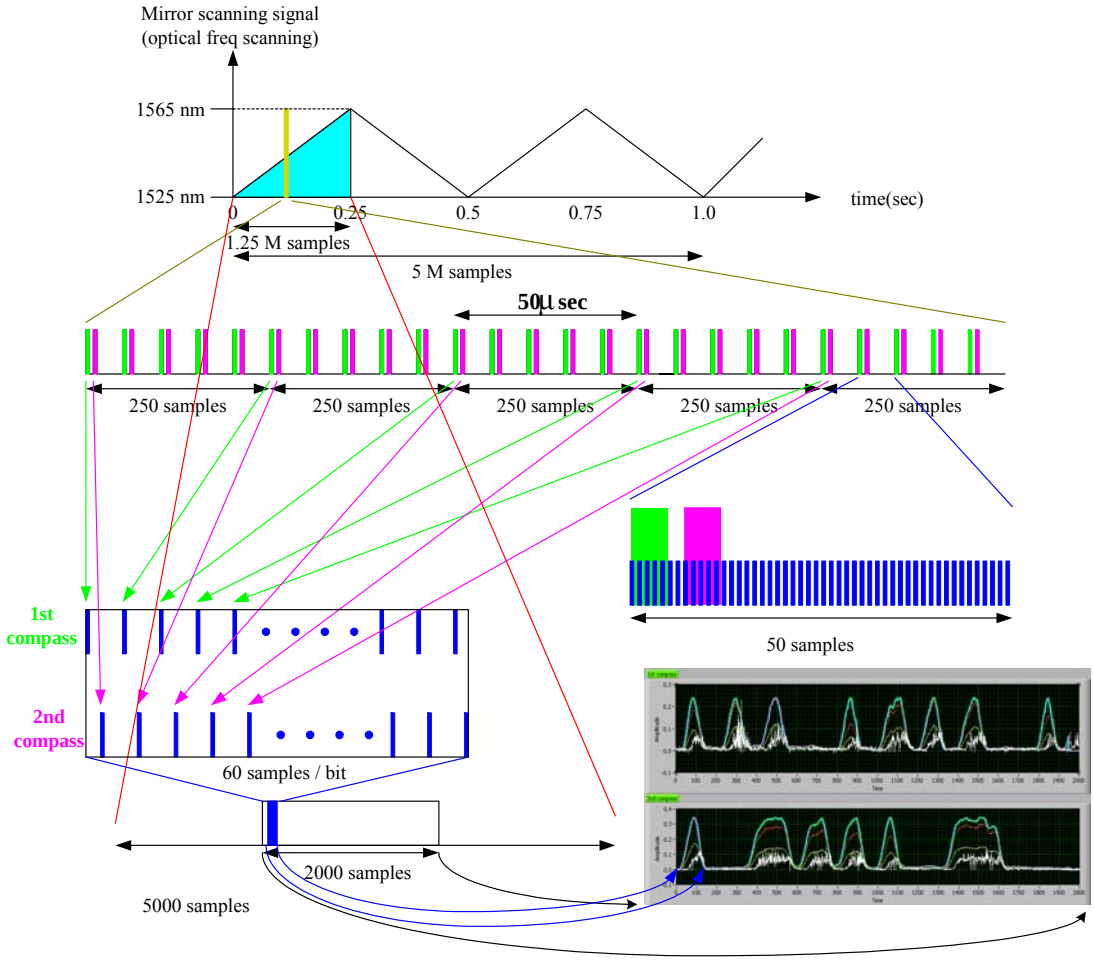

Fig. 6-17. Sample acquisition diagram for two sensor heads

We use a 2 Hz triangular pulse to scan the mirror which is used for wavelength scanning. We just make use of quarter timing of 2 Hz of mirror scanning pulse, so that

we can save the processing time and make it possible to upgrade the compass reading every second. Because the computer processor takes time to acquire samples, we should give the computer marginal time for calculation except just acquisition. Computer is triggered to acquire the samples during first rising time of triangular pulse from two triangular ones, performs the data processing within one data upgrading time and repeats this process.

1.25 M samples are acquired during a quarter second, and 1 sample is selected from every 250 samples for processing to determine the compass readings. Once samples from each sensor head are distributed to the appropriate data blocks in the computer random access memory (RAM), the data for each compass head is processed in parallel by the calculation procedure described in Sections VI. A. through VI. G.. Selected samples for each sensor head are gathered in groups of 60 to make 1 bit width. Then 2000 samples make ~33 bits, which encompass slightly over 2 words.

After sample selection and demultiplexing for each sensor head, the signal processing algorithms are applied to the data from each sensor head reading in the same manner. All sensor head readings are performed at the same time in parallel. Barcode patterns obtained simultaneously from two sensor heads are shown in Fig. 6-18. Processing of these data to obtain heading and pitch information is described in Secs. VI. A. through VI. G. The binary code readings for these two compasses are 0010011 and 0111011.

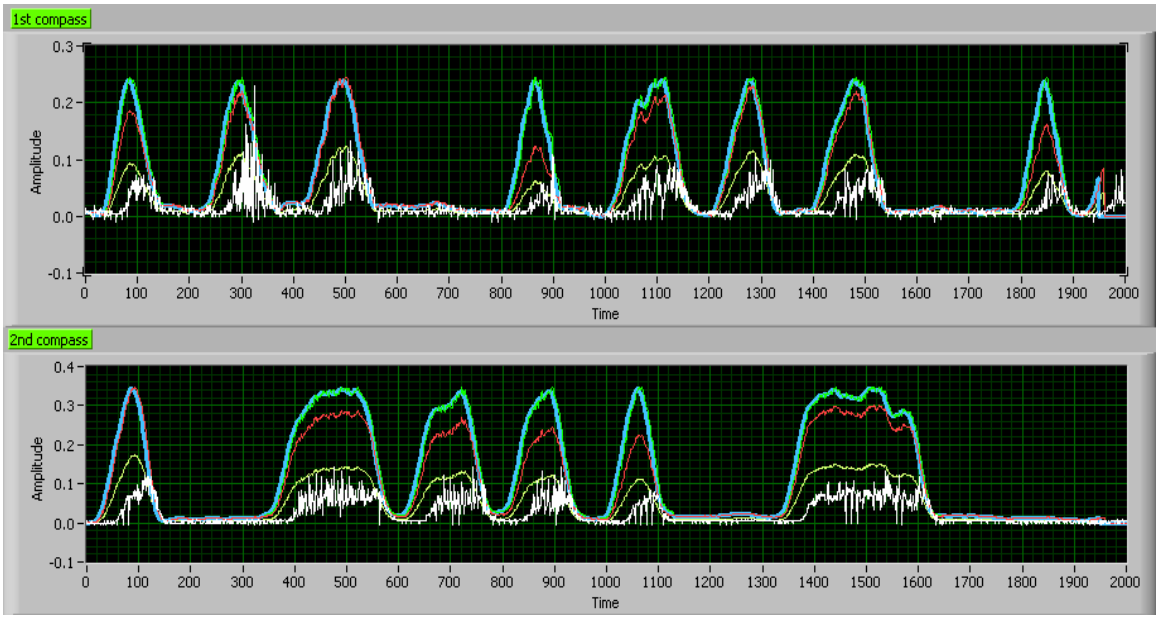

Fig. 6-18. Demultiplexed barcode pattern profiles from 2 sensor heads

VII. TESTING AND PERFORMANCE VERIFICATION

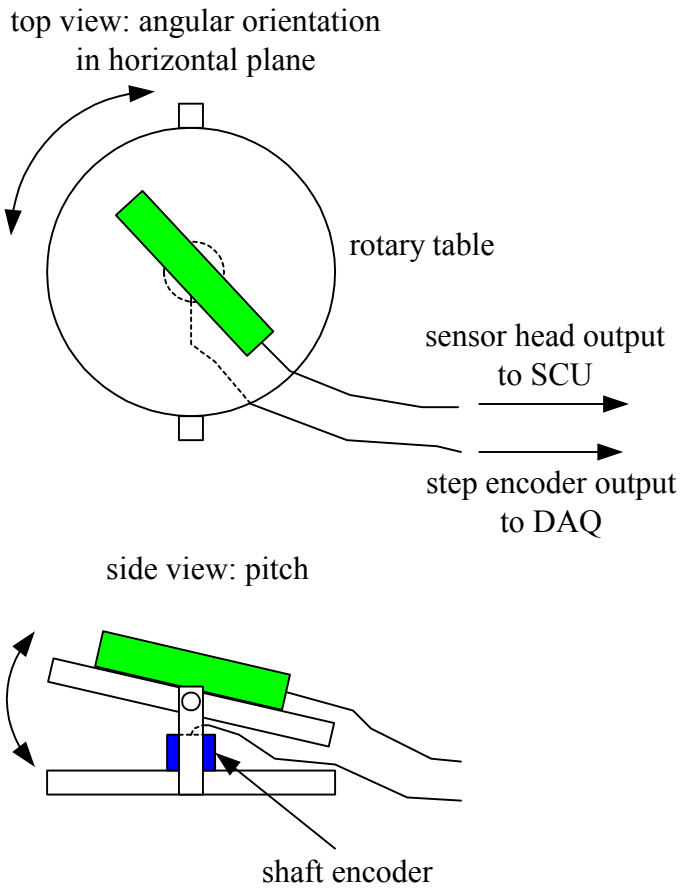

Fig. 7-1. Arrangement for testing of fiber optic compass

To test the compass system's performance, the heading and pitch were varied, and values of these parameters determined with the optical system were compared with calibration values obtained by mechanical position sensing techniques. The cylindrical

sensor head is mounted on a machinist's table for rotating it through 360° in the horizontal plane, as illustrated in Fig. 7-1. In this arrangement, it is also possible to elevate/lower its axis through ±10° to determine the effect of pitch. Data on magnetic heading from the optical system is compared with measurements using a shaft encoder, which has a heading resolution of 0.015º. Pitch is compared with a grid indicator marked on the side of the table. These data is used to evaluate the quality of the barcode patterns and the performance of the signal processing algorithm.

VII. A. Fiber Optic Compass (FOC) Heading Output

To evaluate heading performance through a 360° rotation, the machinist's table is rotated through one turn. During rotation, the DAQ system continuously acquires optical samples for each scanning window, calculates the FOC heading and pitch, and determines the difference between the FOC output and the encoder reading. Because the FS keeps wobbling during rotation of the FOC, the barcode pattern profile from the raw sample data also keeps changing its shape, making it possible to generate errors. Also, defects in the gold barcode pattern are potential error sources.

The FOC heading output for a 360° rotation is shown in Fig. 7-2. As described in Sec. VI. G., the error compensation technique is applied when the FOC heading jumps by more than 30°. The 18 jumps in the raw FOC heading were eliminated by this method.

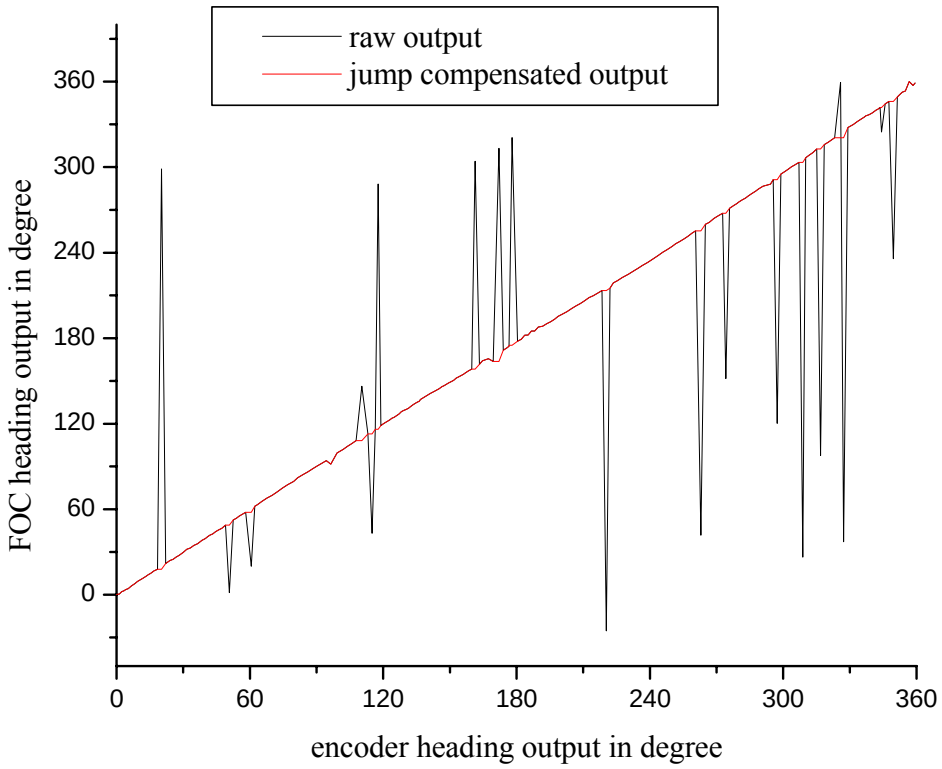

Fig. 7-2. FOC heading output for 360º rotation

To obtain heading readings from the FOC which agree exactly with the encoder readings is very difficult because the FS is manually balanced. Even though FS is well balanced at a stationary position when the magnet is assembled beneath the FS, the FS is inclined to tilt at a certain magnetic direction when it moves and wobble during rotation. If the FS is inclined to a certain direction, the heading changes from the value without tilting. Fig. 7-3 shows the inclination during FOC rotation. The black solid line is the heading difference between FOC and encoder of Fig.7-1. From these data, the FS experiences its greatest inclination in the vicinity of a heading of 240°.

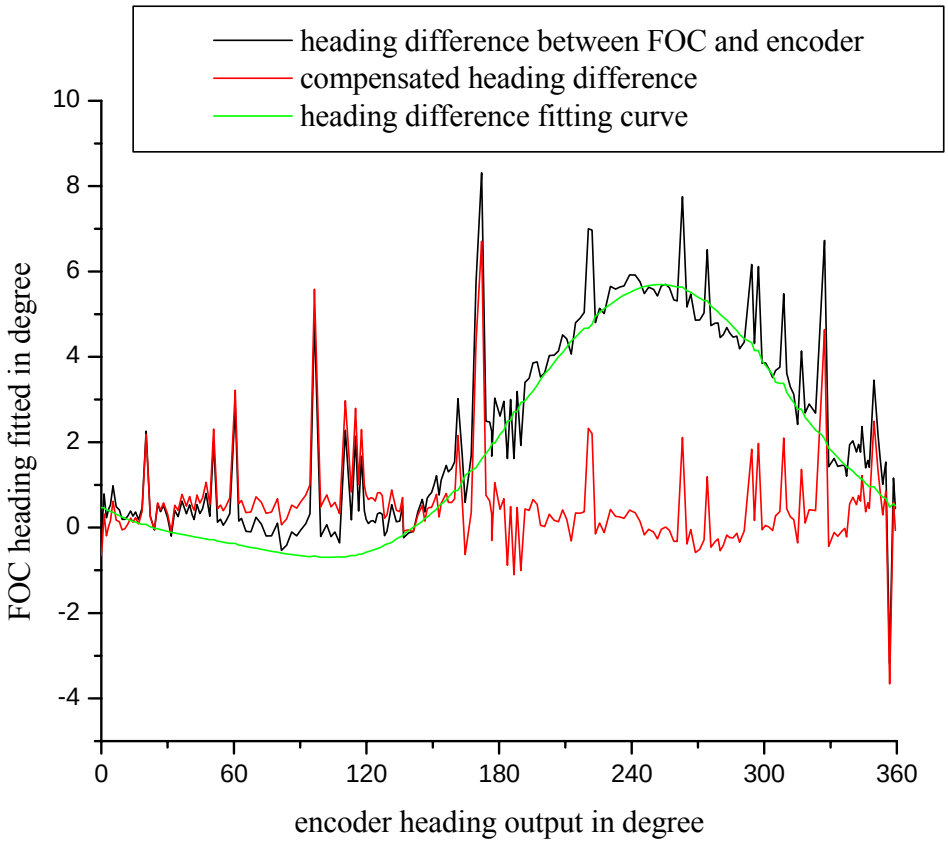

Fig. 7-3. FOC heading adjustment

To compensate for inclination of the FS, we developed a curve for compensating for the difference between FOC and encoder output, given by

$$y = 1.850318 - 2.94490\sin\alpha - 0.933423\cos\alpha + 0.645084\sin 2\alpha - 0.438831\cos 2\alpha \tag{7.1}$$

where y is the curve fitting value for each FOC heading output and α is the FOC heading output in degree.

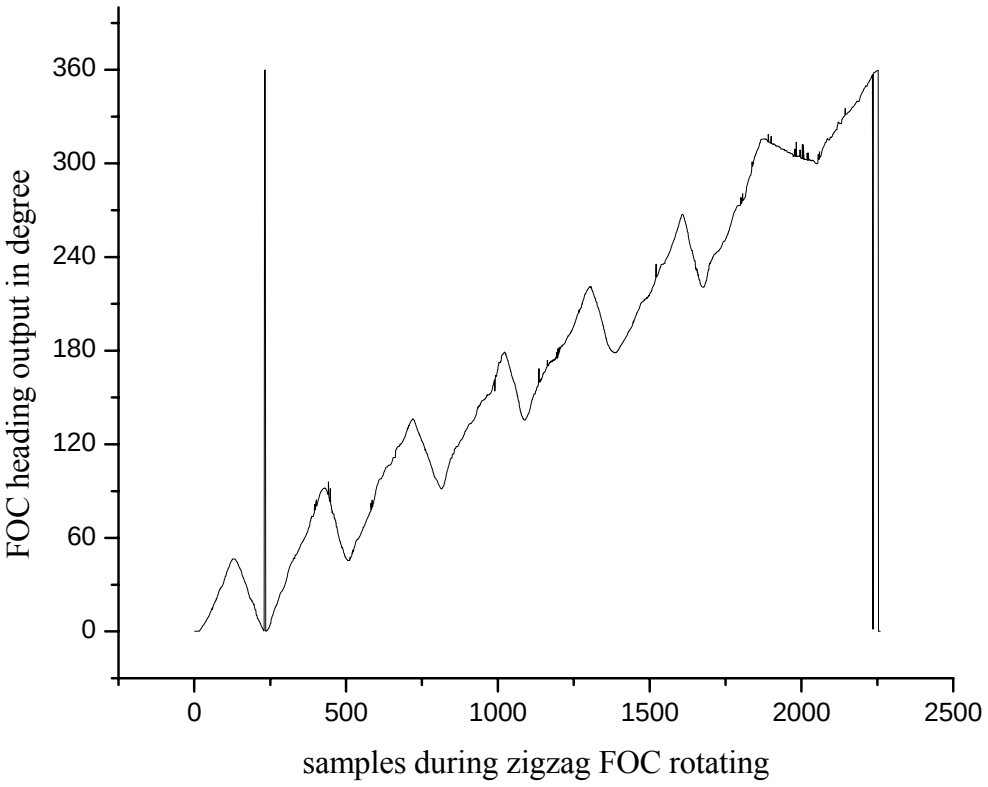

Fig. 7-4. FOC heading measurement during zigzag rotation

The FOC heading was measured and jump compensated during the rotation of the FOC in a zigzag manner, as shown in Fig. 7-4. Fig. 7-4 shows that the FOC is working back and forth in a rotating environment as well as continuous rotation. The heading difference between the FOC and encoder readings after zigzag rotation shows the same pattern as for continuous rotation, as shown in Fig. 7-5, so that heading difference compensation is applicable regardless of the motion of the FOC.

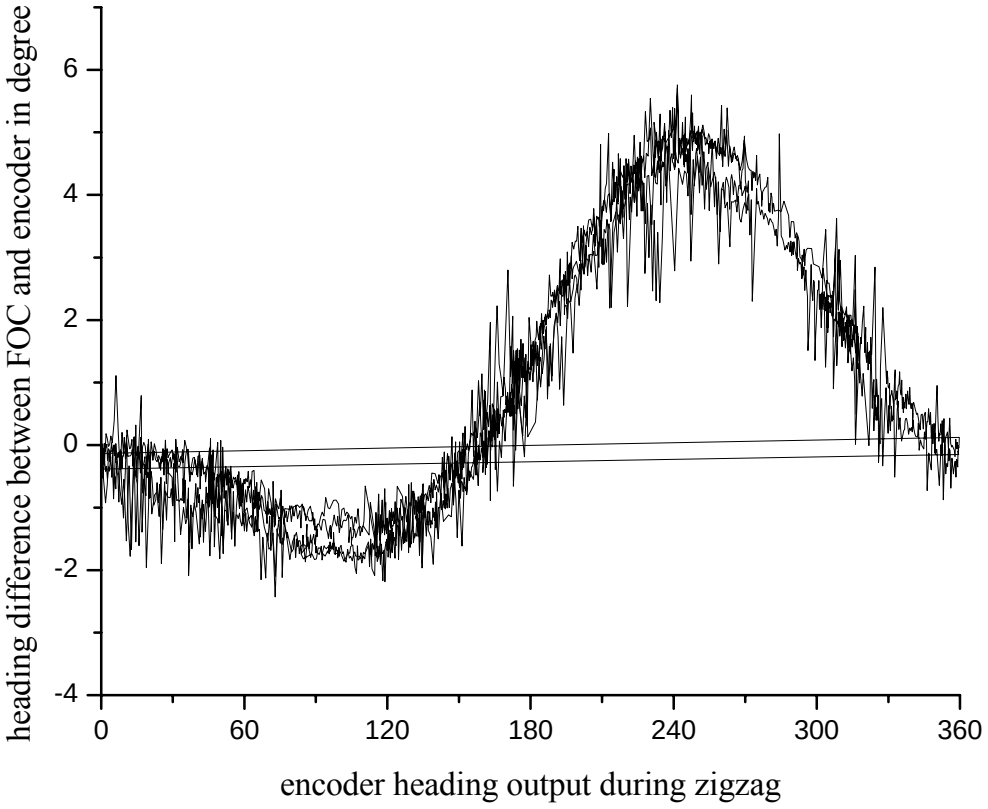

Fig. 7-5. Heading difference after zigzag rotation

VII. B. FOC Pitch Output

The pitch is measured by determining the width of the analog bar. To investigate the pitch measurement performance, the FOC was rotated through 360º at different values of pitch from -5° to 5°. As shown by the data of Fig. 7-6, the FOC pitch output varies with heading of the compass head because FS wobbles during rotation.

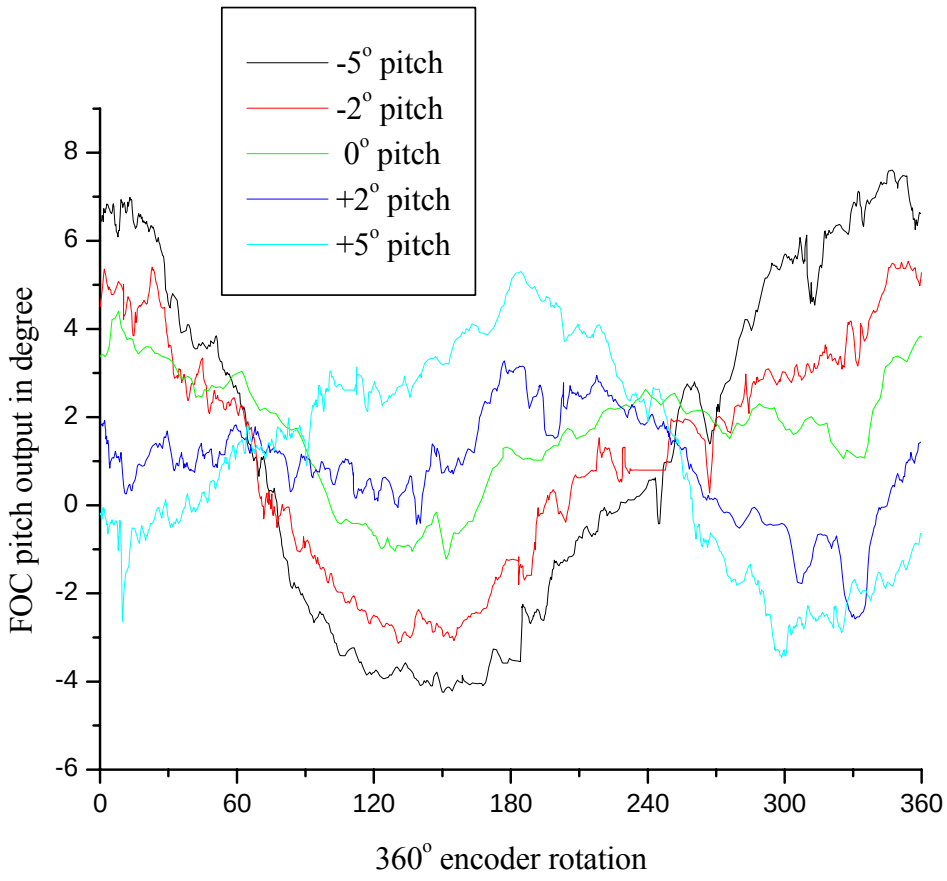

Fig. 7-6. FOC pitch output varying the pitch

For heading measurement, we use the barcode pattern so that the bar width change during scanning is no matter as long as we can determine the bit sequence. In the case of pitch, it is determined absolutely from the measured width of analog bar so that pitch output keeps fluctuating when FS wobbles. Fig. 7-6 shows there are apparent differences between pitches even though each pitch output gets fluctuation. FS inclination also makes the difference between FOC pitch and actual pitch.

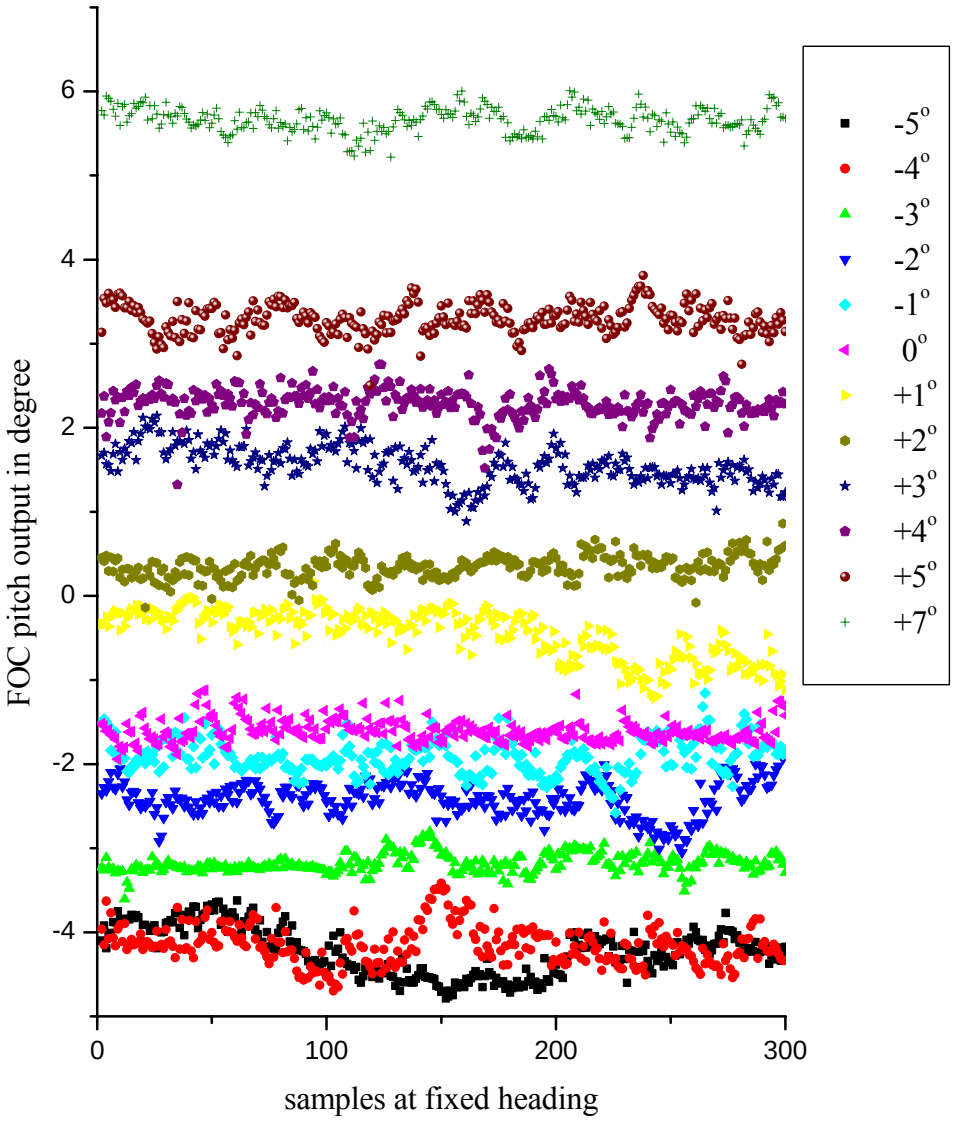

Fig. 7-7. FOC measurement varying pitch at a fixed position

As another indicator of pitch performance, we fixed the FOC heading at 148° and varied the actual FOC pitch from -5º to 7º. The result is shown in Fig. 7-7. At the fixed heading, the pitch fluctuation is much less than for the rotating FOC (Fig. 7-6), because the FS doesn't wobble.

VII. C. FOC Heading and Pitch at Fixed Position

By measuring the fluctuation in measured values of heading and pitch at a fixed position of the compass head, a determination of the resolution of the system can be made.

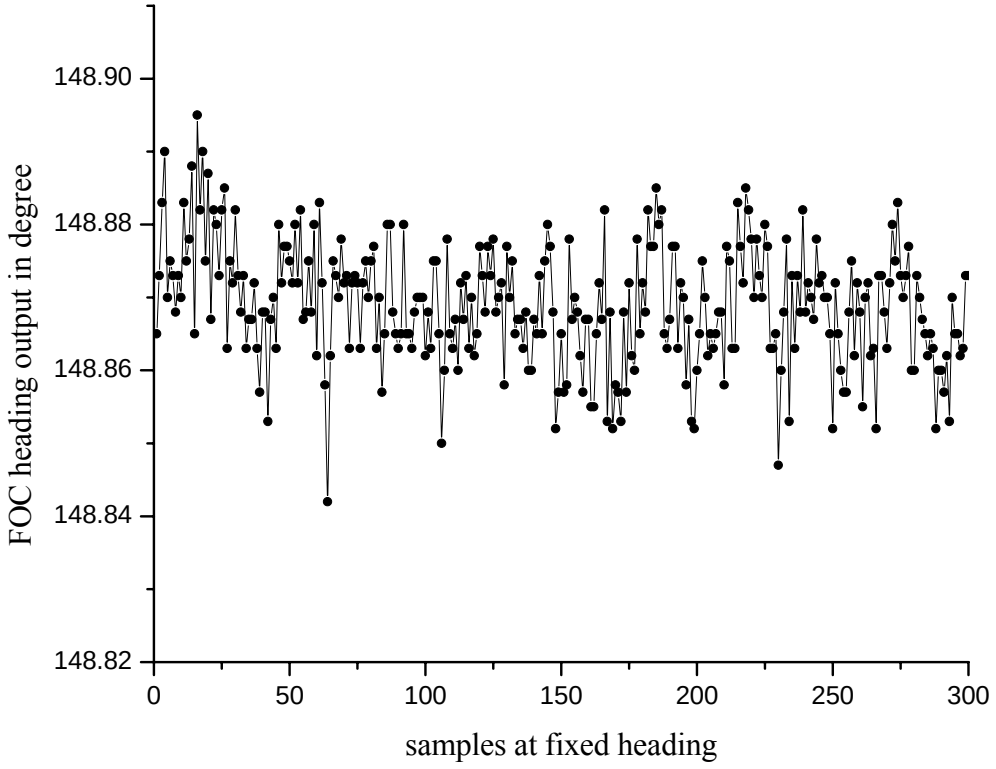

Fig. 7-8. FOC heading output at fixed location

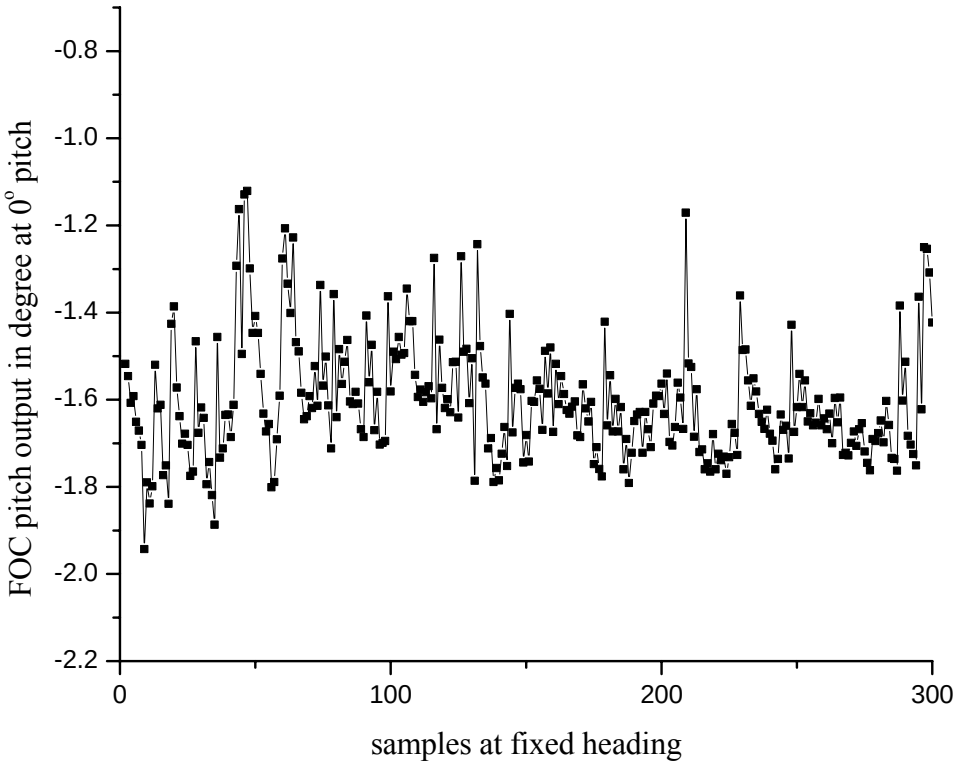

Fig. 7-9. FOC pitch output at fixed location

As indicated earlier, 180 samples are acquired during a bit period, and the resolution corresponding to a single sample is 0.0016667° for heading and 0.037037° for pitch. Fluctuations in the raw sample data cause the sample location for each bar of the scanning window to change as well. The corresponding angular range over which the FOC heading and pitch vary is the actual resolution of the system. From the data of Fig. 7-8, the FOC heading fluctuates over a range of 0.044°, while from the data of Fig. 7-9 the FOC pitch fluctuates over a range of 0.85. In each case the number of samples is 300.

VII. D. FOC Heading Measurement during Slow Rotation of the Compass Head

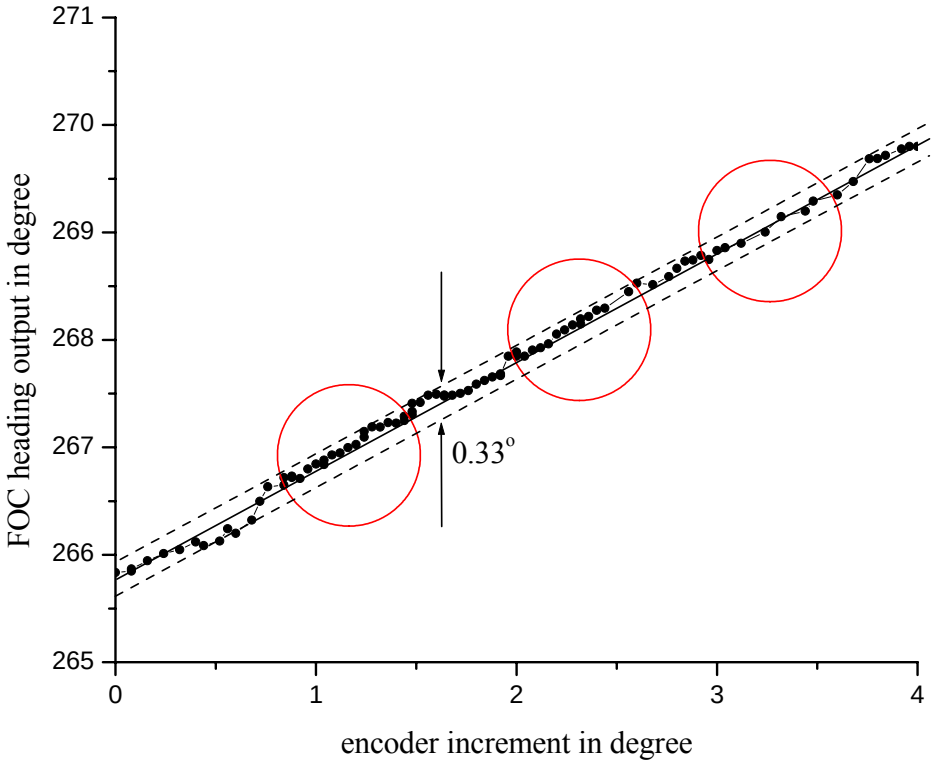

Fig. 7-10. FOC heading output during slow rotation

Fig. 7-10 shows the performance of the system as the compass head is rotated slowly. The possible deviation of the FOC position from the encoder reading due to encoder error is ±0.165°, as shown by the dashed lines in Fig. 7-10. This result is consistent with the value of 0.044° for heading resolution determined from the stationary measurement.

VIII. CONCLUSIONS

Three key aspects of the development of a fiber optic compass system have been addressed in this research: fabrication of a bar code pattern on a floating sphere, data acquisition/signal processing, and system testing and performance verification.

An unconventional photolithographic process for producing a bar-code pattern on a curved (spherical) surface was successfully implemented. First, an absorption process for applying a thin layer of photoresist uniformly to the gold-coated surface of a glass sphere was perfected. Then, a system for defining the patterns in the metal was assembled. This system consists of a high precision (.001°) computer-controlled rotation stage, a mask holder to accommodate a rectangular mask or a triangular mask, a lens for producing a 10x reduced image of a mask onto the surface of the floating sphere, a light source for illuminating the mask in transmission, and a computer-controlled shutter for blocking the light. A LabView computer program controlled the rotating stage and shutter as required to define the bar code pattern in the metal. High-quality bar code patterns were produced on floating spheres by this method.

The data acquisition/signal processing system digitized and processed the raw data returning from the compass heads, and computed magnetic heading and pitch from the data. Processing of the signal from a single compass head required smoothing of the raw data, normalization of the bar code peak heights, identification of a reference point ("fat one") in the pattern, readout of a 7-bit binary code to determine coarse heading,

using timing information to obtain fine heading, and measuring the apparent width of an analog bar to determine pitch. When monitoring multiple compass heads distributed along the fiber, a time-division demultiplexing technique was used for separating the data from the individual compass heads, prior to applying the "single compass head" algorithm described above.

For testing the system, the cylindrical sensor head was mounted on a machinist's table for rotating it through 360° in the horizontal plane to vary the heading, and through ±10° about a horizontal axis to vary pitch. Data on magnetic heading and pitch collected for all possible orientations of the sensor head were compared with actual heading and pitch to determine the fundamental noise level of the fiber optic compass system and its performance. Measured values for the angular resolution of the system were 0.044º for heading, and 0.85º for pitch.

IX. RECOMMENDATIONS FOR FUTURE WORK

IX. A. Roll Pattern Development

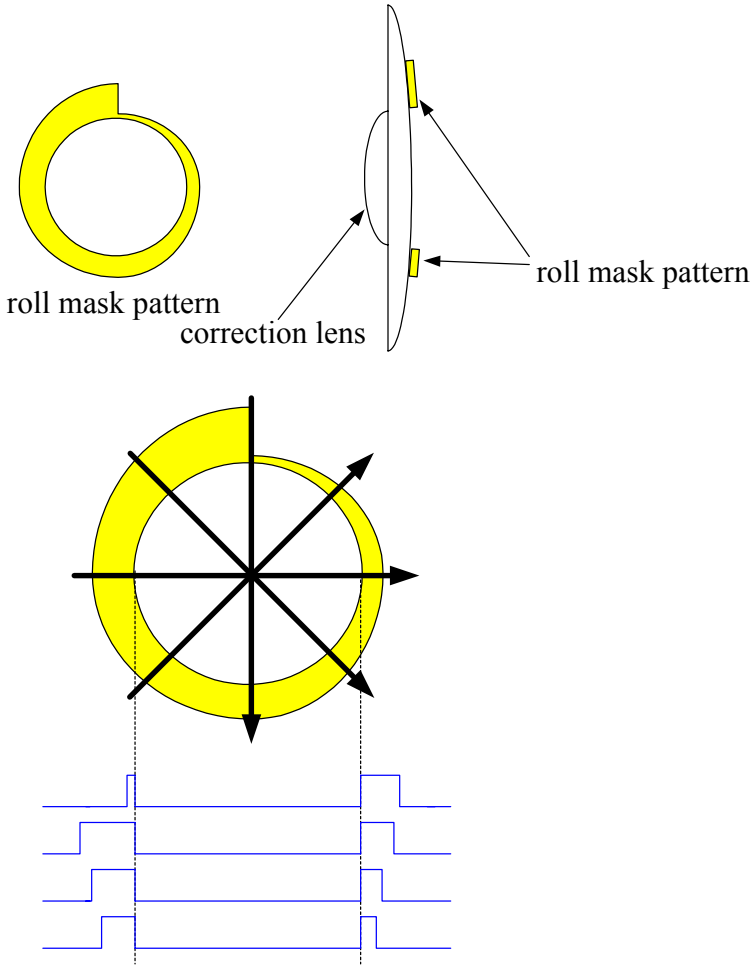

Fig. 9-1. Roll mask pattern on the correction lens

FS contains the heading and pitch information with the barcode pattern composed with 7 digital bars and analog bar for each word. FOC rolling can be obtained by developing a roll mask pattern on the correction lens, as shown in Fig. 9-1, with the photolithography. The radius of curvature of the correction lens can be adjusted so that off-axis rays can be reflected back along their original paths. Because the roll mask pattern is asymmetric in the beam scanned output is unique for each angle from 0° to 360°. The words for measuring heading are confined within the inner circle of the roll mask pattern. To get the width of the roll mask pattern, same algorithm will be used described in Sections VI. A. through VI. G..

IX. B. Surface Recognition Capability

Barcode pattern on FS was successfully read by scanning system. If we replace the FS with any target sample we can also read the surface of the sample with the combination of adequate correction lens to couple back the reflected light. Scanning range of the current setup is 0.78 mm by using a colliminating lens of 5 cm focal length. Scanning rage is subject to the focal length of the colliminating lens. So, a longer focal length can be selected for wide scanning and a shorter for an accurate scanning of the target samples.

REFERENCES

[1] C. E. Lee and H. F. Taylor, "A fiber-optic pressure sensor for internal combustion engines," Sensors, vol. 15, p. 20, no. 3, March 1998.

[2] E. Udd, *Fiber-optic Sensors*, New York: Wiley, 1991

[3] M. N. Deeter, "Magneto-optic magnetic field sensor with 1.4 pT/Hz1R minimum detectable field at 1 kHz," *Elec. Lett*. vol. 29, pp. 993-994, May 1993.

[4] K. B. Rochford, A. H. Rose and G. W. Day, "Magneto-optic sensors based on iron garnets," *IEEE Trans. Magn.* vol. 32. pp. 4113-4117, Sept. 1996

[5] K. B. Rochford, R. J. Espejo, A. H. Rose and S. D. Dyer, "Improved fiber-optic magnetometer based on iron garnet crystals," in *Proc., 14th Optical fiber sensors conf.*, Venice, Italy, Oct. 11-13, pp. 332-335, 2000

[6] A. Dandridge, A. B. Tveten, G. H. Sigel, Jr., E. J. West and T. G. Giallorenzi, "Optical fiber magnetic field sensors," *Electron. Lett*. vol. 16, pp. 408-409, Apr. 1980.

[7] A. R. Davis, S. S. Patrick, A. Dandridge, and F. Bucholtz, "Remote fibre-optic AC magnetometer," *Electron. Lett*., vol. 28, pp. 271-273, Jan. 1992.

[8] K. P. Koo and G. H. Sigel, Jr., "Characteristics of fiber-optic magnetic-field sensors employing metallic glasses," *Opt. Lett*., vol. 7, pp. 334-336, July 1982.

[9] K. P. Koo, A. Dandridge, A. B. Tveten and G. H. Sigel, Jr. , "Fiberoptic dc magnetometer," *J. Lightwave Technol*. , vol. LT-1, no. 3, pp. 524-525, 1983.

[10] J. E. Livingston, "Magnetomechanical properties of amorphous metals," *Phys. Stat. Sol*., vol. 70, pp. 591-596, June 1982

[11] X. Wan and H. F. Taylor, "Linearly chirped erbium-doped fiber laser," *IEEE Photon. Technol. Lett.*, vol. 15, pp.188-189, Feb. 2003

[12] X. Wan and H. F. Taylor, "Fiber-Bragg-grating pair interferometer sensor with improved multiplexing capacity and high resolution," *IEEE Photon. Technol. Lett.*, vol. 15, pp.742-744, May 2003

[13] S. M. Sze, *VLSI Technology*, McGraw-Hill, New York, 1983

[14] L. F. Thompson, C. G. Wilson, and M. J. Bowden, *Introduction to Microlithography*, American Chemical Society, Washington, D.C., 1983

VITA

Kyongtae Park was born in Sokcho, Republic of Korea in 1971. He received his B.S. and M.S. degrees in electronic engineering from Kangwon National University in 1997 and 1999 respectively. In January 2000, he was admitted to the graduate school at Texas A&M University. He received his Ph.D. degree in electrical engineering at Texas A&M University in 2004. His major interests include optical pickup, fiber optic sensor, optical signal processing and optical communications. He can be reached at the following address:

Kyongtae Park

488-259 Kumho-dong Sokcho-si

Kangwon-do 217-040, Korea

E-mail: jdmpkt@hanmail.net